ABSTRACT

Title of Dissertation: An Octahedral Tiling on the Ideal Boundary of the Complex Hyperbolic Plane

Blake P. Pelzer, Doctor of Philosophy, 2006

Dissertation directed by: Professor Richard Schwartz
Department of Mathematics
Brown University

We present an octahedral tiling on the ideal boundary of the complex hyperbolic plane. The tiling was discovered through use of a program we wrote called CHAT. We show visual evidence of this tiling and prove some results about embedding a specific tile.

An Octahedral Tiling on the Ideal Boundary of the Complex Hyperbolic Plane

by

Blake P. Pelzer

Dissertation submitted to the Faculty of the Graduate School of the
University of Maryland, College Park in partial fulfillment
of the requirements for the degree of
Doctor of Philosophy
2006

Advisory Committee:

Professor Richard Schwartz, Chairman
Professor William Goldman
Professor John Millson
Professor David Mount
Professor Clyde Kruskal

TABLE OF CONTENTS

LIST OF TABLES

LIST OF FIGURES

Chapter 1

Introduction

The complex hyperbolic plane is a four-dimensional symmetric space of negative curvature. A complex hyperbolic triangle group is an isometry group generated by three complex reflections (Definitions are given below.) Goldman and Parker introduced these groups in the early 1990's, and several authors have addressed them in the intervening years. In particular, Richard Schwartz classified, in terms of discreteness, the 1-parameter family of so-called ideal complex hyperbolic triangle groups. This classification answered a conjecture posed by Goldman-Parker. Our focus in this thesis will be the so-called last discrete complex hyperbolic triangle group, which appears at the nontrivial end of the 1-parameter family of ideal complex hyperbolic triangle groups

In this thesis we examine a pattern of topological triangles on the boundary of $\mathbb{C}H^2$. We obtained this pattern through extensive computer simulations using a program we wrote for this purpose. The triangles arise from objects adapted to the (∞, ∞, ∞) triangle group, using the boundary components of geodesic subspaces in complex hyperbolic space. We hope that this pattern will eventually help to explain this group action.

I would like to express my gratitude to Richard Schwartz for steering me into

the field and the problem. I would also like to thank Bill Goldman for his support and guidance.

1.1 Summary of Results

This dissertation has four chapters. The first covers the necessary background material for complex hyperbolic triangle groups. The second deals with the use and structure of CHAT, a program we created to visualize objects on the ideal boundary of $\mathbb{C}H^2$. In the third chapter, we present empirical evidence, obtained from CHAT, to support the existence of an octahedral tiling. Lastly we prove some embedding results for an octahedron in the tiling.

CHAT is designed to draw and manipulate triangles in $\partial\mathbb{C}H^2$. In the second chapter we provide instructions for the reader to use the program. An example is included to familiarize the user with the interface. Additionally, we describe CHAT's construction and methods one may use to program abstract results. We conclude with a detailed explanation of the projections used to produce two dimensional images.

Chapter 3 contains convincing visual evidence produced by CHAT to show that there is a tiling by embedded octahedra. We select a specific octahedron, discuss its symmetries, and choose representatives from each class of face pairings. We give detailed pictures to support that each pair of faces is embedded. Lastly, we show images of the octahedron in relation to certain spheres in $\partial\mathbb{C}H^2$. This collection of images substantiates the claim that the selected octahedron produces a tiling.

Our goal is to show that the tiling is embedded, and chapter 4 offers partial results to support this hypothesis. We show that the octahedron consists of two

embedded halves and prove some results about their union near their common vertices. The chapter begins with a discussion of some parameterizations of common objects in $\mathbb{C}H^2$. We then employ those tools to ascertain that half of the octahedron is embedded. We also show, modulo roundoff error, that the two halves are embedded near two of their joining vertices, and prove that most of the faces are embedded near the other two vertices.

1.2 Background

To obtain the complex hyperbolic plane $\mathbb{C}H^2$, we begin with $\mathbb{C}^{2,1}$, i.e. three dimensional complex space with the hermitian form $\langle \quad , \quad \rangle$ given by

$$\langle z, w \rangle = z_0\bar{w}_0 + z_1\bar{w}_1 - z_2\bar{w}_2$$

This breaks $\mathbb{C}^{2,1}$ into three regions, positive $\{z \in \mathbb{C}^{2,1} : \langle z, z \rangle > 0\}$, negative $\{z \in \mathbb{C}^{2,1} : \langle z, z \rangle < 0\}$, and null $\{z \in \mathbb{C}^{2,1} : \langle z, z \rangle = 0\}$. $\mathbb{C}H^2$ is the projective image of the negative region in $\mathbb{C}P^2$, which we identify with the open unit ball in $\mathbb{C}^2$. The ideal boundary, $\partial\mathbb{C}H^2$, is the projectivization of the null region, which we identify with $S^3 \subset \mathbb{C}^2$. For any $x \in \mathbb{C}H^2$ we will denote any lift of x by $\tilde{x}$. The holomorphic isometry group of $\mathbb{C}H^2$ is $PU(2,1)$. There are three fundamental categories for elements of $PU(2,1)$. Elliptic elements fix at least one point in $\mathbb{C}H^2$, but may fix points on the boundary as well. Parabolic elements have a unique fixed point and it lies in $\partial\mathbb{C}H^2$. Lastly, hyperbolic elements fix two points in $\partial\mathbb{C}H^2$. [Go] is an excellent resource for facts about $\mathbb{C}H^2$.

There is an important invariant of three points in $\partial\mathbb{C}H^2$.

Definition 1.2.1. *Given three points, x, y, and p, in $\partial\mathbb{C}H^2$, their* ***angular***

invariant *is given by:*

$$\arg(-\langle \tilde{x}, \tilde{y}\rangle \langle \tilde{y}, \tilde{p}\rangle \langle \tilde{p}, \tilde{x}\rangle) \in [-\frac{\pi}{2}, \frac{\pi}{2}]$$

If three points lie on a common geodesic in $\partial \mathbb{C}H^2$, their angular invariant will be 0 if the geodesic is real and $\pm\frac{\pi}{2}$ if it is complex. For more information, see [Go] pp.210-214.

The abstract (p, q, r) triangle group has the presentation:

$$\langle I_0, I_1, I_2 \quad | {I_0}^2 = {I_1}^2 = {I_2}^2 = (I_0 I_1)^p = (I_1 I_2)^q = (I_2 I_0)^r = Id \rangle$$

This presentation mimics the geodesic real hyperbolic triangle with angles $(0, 0, 0)$. In our case we are interested in $p = q = r = \infty$, isomorphic to $\frac{\mathbb{Z}}{2} * \frac{\mathbb{Z}}{2} * \frac{\mathbb{Z}}{2}$. We denote this group by $\triangle$. In order to define a representation of $\triangle$ into $\mathbf{Isom}(\mathbb{C}H^2)$, we must define what object we are reflecting through, and how we carry out the reflection.

Definition 1.2.2. *Let $x, y \in \mathbb{C}H^2 \cup \partial \mathbb{C}H^2$. Let $\tilde{C}$ be the complex span of $\tilde{x}$ and $\tilde{y}$ in $\mathbb{C}^{2,1}$. We define the* ***complex slice*** *C containing x and y by projectivizing $\tilde{C}$ and then intersecting with $\mathbb{C}H^2 \cup \partial \mathbb{C}H^2$. C is a complex 1-dimensional submanifold.*

We need two more definitions to proceed. The first is an operation analogous to the cross product in Euclidean space. This will enable us to find a vector orthogonal to our complex slice.

Definition 1.2.3. *The* ***Box Product***

$$\boxtimes : \mathbb{C}^{2,1} \times \mathbb{C}^{2,1} \to \mathbb{C}^{2,1}$$

is defined by

$$u \boxtimes v = (\overline{u_3v_2 - u_2v_3}, \overline{u_1v_3 - u_3v_1}, \overline{u_1v_2 - u_2v_1})$$

Definition 1.2.4. *The **polar vector**, unique up to scaling, for a complex slice C is the vector $\tilde{x} \boxtimes \tilde{y}$ where $\tilde{C} = span(\tilde{x}, \tilde{y})$.*

A quick calculation shows that $\langle \tilde{x} \boxtimes \tilde{y}, \tilde{y} \rangle = 0$.

$$\begin{aligned} \langle \tilde{x} \boxtimes \tilde{y}, \tilde{y} \rangle &= (\overline{x_3y_2 - x_2y_3})\bar{y_1} + (\overline{x_1y_3 - x_3y_1})\bar{y_2} - (\overline{x_1y_2 - x_2y_1})\bar{y_3}) \\ &= \overline{x_3y_2y_1} - \overline{x_3y_1y_2} + \overline{x_2y_1y_3} - \overline{x_2y_3y_1} + \overline{x_1y_3y_2} - \overline{x_1y_2y_3} \\ &= 0 \end{aligned} \tag{1.1}$$

and similarly that $\langle \tilde{x} \boxtimes \tilde{y}, \tilde{x} \rangle = 0$. Moreover, this definition does not depend on the lifts of x and y, since different lifts will result only in a different scaling of the vector.

Now we are in a position to calculate the reflection in a complex slice.

Definition 1.2.5. *The **complex reflection** in C is given by*

$$I_C(\tilde{u}) = -\tilde{u} + \frac{2\langle \tilde{u}, \tilde{p} \rangle}{\langle \tilde{p}, \tilde{p} \rangle} \tilde{p}$$

where p is the polar vector for the complex geodesic C.

Now if we choose three distinct points, v_0, v_1, v_2, in $\partial \mathbb{C}H^2$ then each pair will define a polar vector for a complex slice. Let C_0, C_1, and C_2 denote the complex slices determined by the pairs $\{v_0, v_2\}$, $\{v_1, v_2\}$, and $\{v_0, v_1\}$ respectively. We can then define a representation

$$\rho : \triangle \to PU(2,1)$$

by mapping each generator to the complex reflection in the slice with corresponding index. The deformation space of such representations has one real dimension. The main result of [S0] is that such a representation is discrete and faithful if and only if the element $I_0I_1I_2$ is not elliptic. The discrete embeddings can then be parameterized by the closed interval, $[0, \sqrt{\frac{125}{3}}]$, up to conjugation. This parameter has a geometric significance described on page 18. We define Γ to be the image of the representation given by the parameter $\sqrt{\frac{125}{3}}$ where the element $I_0I_1I_2$ is parabolic. This is the last faithful, discrete (∞, ∞, ∞) triangle group.

There are two kinds of totally geodesic subspaces in $\mathbb{C}H^2$. We have already defined one, the complex slice. Its boundary will be of great interest to us, as will the other kind of subspace.

Definition 1.2.6. *The accumulation set of a complex slice on $\partial\mathbb{C}H^2$ is a* $\mathbb{C}$***-circle**. A segment of a $\mathbb{C}$-circle will be called a* $\mathbb{C}$***-arc***

Definition 1.2.7. *A* ***real slice*** *is a totally real, totally geodesic subspace of $\mathbb{C}H^2$. An* $\mathbb{R}$***-circle*** *is the accumulation set of a real slice on $\partial\mathbb{C}H^2$.A segment of an $\mathbb{R}$-circle will be called an* $\mathbb{R}$***-arc**. All real slices are isometric to $\mathbb{R}^2 \cap \mathbb{C}H^2$.*

Given two distinct points on $\partial\mathbb{C}H^2$, there is a unique $\mathbb{C} - circle$ that contains them. Every example is $PU(2,1)$ equivalent to $\mathbb{C}\times 0 \cap \partial\mathbb{C}H^2$. Two distinct points in $\partial\mathbb{C}H^2$ do not specify a unique $\mathbb{R}$-circle, however. Instead, they determine a 1-parameter family of $\mathbb{R}$-circles. To obtain a specific circle, B, in this family we require a third point that lies on B.

There is another setting, permitting easier visual analysis, for $\partial\mathbb{C}H^2$. By removing a point, x, from $\partial\mathbb{C}H^2$ and realizing that $\partial\mathbb{C}H^2$ is homeomorphic to S^3, we can map $\partial\mathbb{C}H^2 - \{x\}$ to Heisenberg space, $\mathcal{H}$, via Heisenberg stereographic

projection (defined below.) Heisenberg space is the set $\mathbb{C} \times \mathbb{R}$ equipped with the group law:

$$(z_1, t_1) \cdot (z_2, t_2) = (z_1 + z_2, t_1 + t_2 + 2Im(\bar{z}_1 z_2))$$

This setting is advantageous because Heisenberg stereographic projection, an analogue of the familiar stereographic projection, is a projective transformation. In particular, any element of $\mathbf{Isom}(\mathbb{C}H^2)$ fixing x gives rise to an automorphism of $\mathcal{H}$. Henceforth we will use the term "stereographic projection" to mean Heisenberg stereographic projection. Here is a standard example of Heisenberg stereographic projection from $S^3 - \{(1, 0)\}$.

$$(z, w) \mapsto (\frac{z}{1+w}, -Im(\frac{1-w}{1+w})$$

A $\mathbb{C}$-circle through our point x maps to a vertical line in $\mathcal{H}$, and we can choose an appropriate stereographic projection to make it the line $\{0\} \times \mathbb{C}$. An $\mathbb{R}$-circle through x maps to a horizontal line, i.e. it will have constant t-value in $\mathcal{H}$. The appropriate projection will make it the line $\mathbb{R} \times \{0\}$.

Before defining our tiling, we must describe its location. The *limit set*, Λ of our group Γ is the accumulation set on S^3 of any orbit $\Gamma(x)$ for any x in $\mathbb{C}H^2$. The limit set does not depend on the choice of x. The *domain of discontinuity* of Γ is the complement, $\Delta = S^3 - \{\Lambda\}$. The tiling is a subset of Δ that is invariant under the action of Γ. Each tile is, experimentally, an embedded octahedron with an order 4 symmetry group.

The triangular faces of an octahedron in our tiling are composed of a single $\mathbb{C}$-arc and many $\mathbb{R}$-arcs. Suppose we have a $\mathbb{C}$-arc and a point q not on it. We wish to connect every point of the $\mathbb{C}$-arc to q by an $\mathbb{R}$-arc, thus making a triangle. To accomplish this, we must utilize additional data. The following definition will

provide the extra data required.

Definition 1.2.8. *A **flag** is a pair (E, q), where E is a $\mathbb{C}$-circle stabilized by an element $\gamma \in \Gamma$ and q is a point on E fixed by γ.*

1.2.1 The Coning Process

Finally, we must define the coning construction that creates the surface of a triangular face. This construction was developed in [S0]. Given a point p on a $\mathbb{C}$-arc and a flag (E, q) with $p \notin E$, there is a unique $\mathbb{R}$-circle, R through p and q that intersects E at another point, z, distinct from q. R is divided into three arcs by p, q, and z, and we select the arc containing p and q but not z for our face. Repeating this procedure for all the points on a $\mathbb{C}$-arc yields a topological triangle, foliated by $\mathbb{R}$-arcs. Every face of our octahedron is such a triangle.

Lemma 1.2.1. *Let p be a point on a $\mathbb{C}$-arc and let (E, q) be a flag, with $p \notin E$. Then there is a unique $\mathbb{R}$-circle, R, such that $R \cap E - \{p, q\} \neq \emptyset$.*

Proof. Consider a Heisenberg stereographic projection of $S^3 - \{q\}$ to $\mathcal{H}$ mapping E to $0 \times t$. Under this mapping, all $\mathbb{R}$-circles through q will be horizontal lines. In particular, any horizontal line through p will be an $\mathbb{R}$-circle through q. There will be exactly one of these lines that intersects the t-axis. This intersection point is z, which lies on both the $\mathbb{R}$ circle and E. Also, z is distinct from q. □

Given a $\mathbb{C}$-arc, C, and a flag (E, q) disjoint from C, the *triangle* with base C is the surface formed by coning each point of C to q by the above construction. The resulting surface is foliated by $\mathbb{R}$-arcs. Such triangles are the faces of our tiling octahedra.

Chapter 2

The Program

2.1 Preliminaries

In the last chapter, we described how three points on the boundary of $\mathbb{C}H^2$ can be used to determine the representation of our triangle group. These three points, v_0, v_1, v_2 are also critical in specifying the triangles in our tiling. Recall that C_0, C_1, and C_2 denote the complex slices determined by the pairs $\{v_0, v_2\}$, $\{v_1, v_2\}$, and $\{v_0, v_1\}$ respectively. For each of the three complex slices C_0, C_1, C_2, there is a $\mathbb{C}$-circle boundary, and each one of these contains two of our three boundary points. Accordingly, each $\mathbb{C}$-circle is divided into two $\mathbb{C}$-arcs joined at these two points. As we will only be concerned with the circles, we will henceforth use C_0, C_1, C_2 to denote the $\mathbb{C}$-circles rather than the complex slices that they bound.

There is another transformation in $PU(2,1)$ that will be helpful to us. This element has order three and cyclically permutes the three defining points v_0, v_1, v_2 and therefore permutes C_0, C_1, and C_2. We shall call this element σ. The orbit of σ is $v_0 \to v_2 \to v_1$.

We must now differentiate the two arcs of a given $\mathbb{C}$-circle. Consider the $\mathbb{C}$-circle C_1. We define the *short* and *long* arcs of C_1 relative to the flag (E, q) by

the following procedure. Take a map from $S^3 - \{q\}$ to $\mathcal{H}$ sending E to the t-axis. Then observe the images of the two arcs under this map and the projection $(z, t) \mapsto z$. One of these arcs will be a sector of angle greater than π. This arc we define to be *long*. The remaining arc is *short*. For C_2 and C_0, we define the *long* arcs by the images of the *long* arc of C_1 under the maps σ, σ^2 respectively. The *short* arcs are determined similarly. We will denote by C_i *long* and C_i *short* the arcs defined relative to the flag for the element $I_1 I_0 I_2$.

2.2 An Overview of CHAT

Recall that we form a triangle from a $\mathbb{C}$-arc, and a flag (E, q) associated to an element of Γ by the coning procedure defined in the previous chapter. We will say that the $\mathbb{C}$-arc, C is coned to the fixed point, p, of $\gamma \in \Gamma$ to describe the construction of a triangle T from C and the flag for γ. We will refer to p as the cone point for T. We will write C *short* $\rightarrow p_{jkl}$ to denote the triangle formed from the short arc of C and the flag associated to the element $I_j I_k I_l$. We now explain the program CHAT that draws these triangles, enabling us to find the octahedral tiling.

A copy of CHAT is available at http://www.math.umd.edu/∼bpelzer. Instructions for running CHAT are found in a README file in the directory containing the program. Running the program launches a window labeled CHAT.This window has three horizontal panes: the menu bar, the display, and the log, from top to bottom respectively. The user selects a triangle with the left half of the menu bar, then views the triangle in the display and its label in the log pane. The right half of the menu bar is primarily for manipulating drawn triangles. Figure 2.1 shows an approximation of the main window that the user will see.

Below is a list of the functions and capabilities of CHAT. The user can:

- Choose a $\mathbb{C}$-arc base and a cone point
- Choose a word in the group Γ and apply it to a triangle
- Select two colors to use when displaying the triangle
- Select a coordinate system to view the triangles
- Save images, generate a tiling, and toggle between displaying surfaces or arcs
- Zoom in or out on a displayed region
- Show, hide, or erase triangles in the display

We will explain each item in a new subsection.

2.2.1 Choosing $\mathbb{C}$-arcs and cone points

Looking at figure 2.1, we see that the menu bar is immediately underneath the window title "CHAT." The leftmost control on the menu bar is a button labeled "Triangle." Clicking on "Triangle" with the left mouse button launches a new window. The left column in this window present a list of potential $\mathbb{C}$-circles and group elements. Clicking on an item in this column selects the $\mathbb{C}$-circle fixed by the named element. For example clicking on "I0 coned to ..." selects the $\mathbb{C}$-circle fixed by the element I_0. The additional number in each item specifies an element γ in the group whose flag will be used in the coning process. The fixed point of γ will be the cone point of the resulting triangle. For example, "I0 coned to 102"

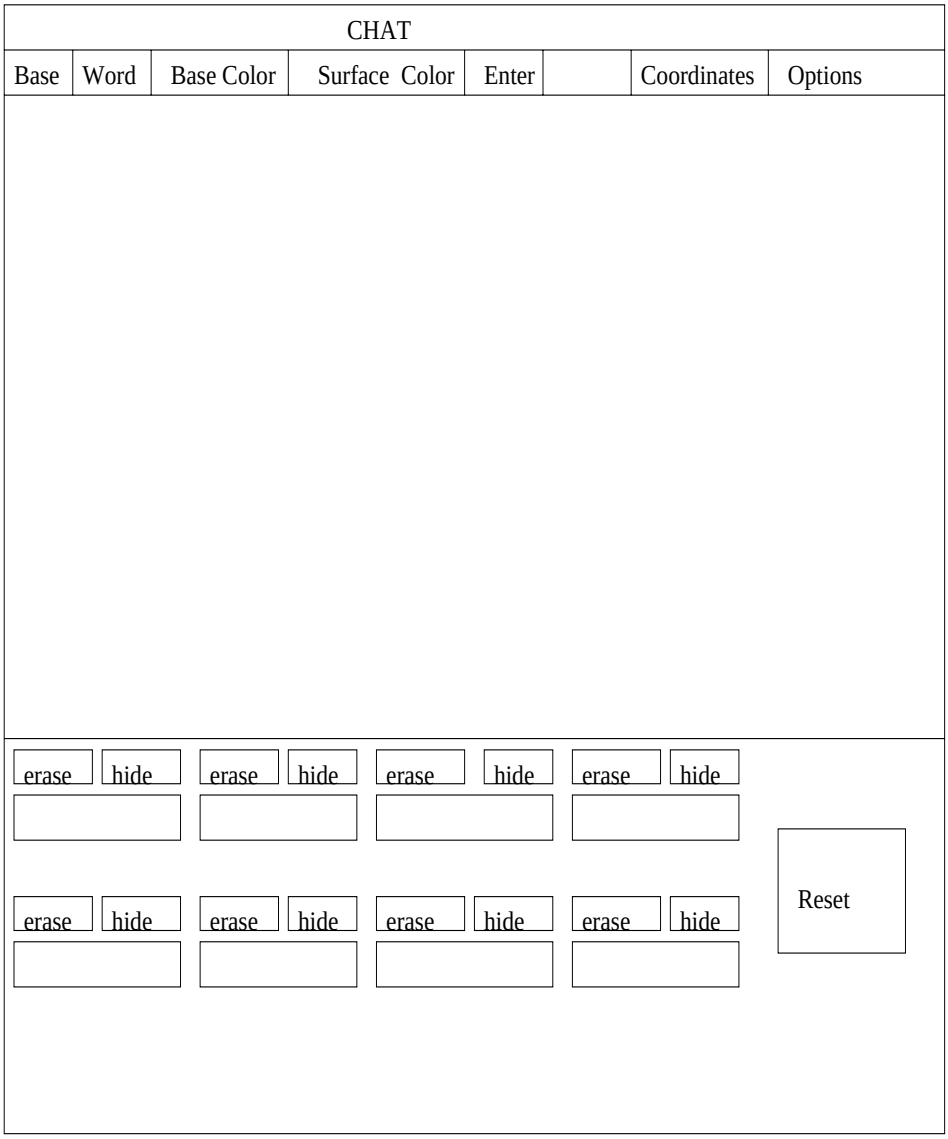

Figure 2.1: A representation of the interface for CHAT

selects the $\mathbb{C}$-circle fixed by I_0 as the base and $\mathbb{R}$-arcs coning from it to the fixed point of the element $I_1 I_0 I_2$ as the surface.

The second column in this window has two options: "Short Arc" and "Long Arc." Clicking on one of these selects a side of the specified $\mathbb{C}$-circle. Practically, the left column determines the three vertices of the triangle while the right determines the base. The coning process determines the rest of the triangle. Once the selections have been made, clicking on the blue "Enter" button confirms them and closes the window.

2.2.2 Choosing a word

The next button in the menu bar is labeled "Word." Clicking on this button launches a new window titled "Word Entry," that allows you to type in a word in the group using the keyboard. This word will then be applied to the triangle. Valid entries are the numbers 0, 1, 2, and 3. The numbers 0, 1, and 2 represent the generators I_0, I_1, and I_2, while 3 represents the map σ. A set of these numbers represents a composition in the generators of the group and the transformation σ. For example typing the word "0123" will specify that the composition $I_0 I_1 I_2 \sigma$ should be applied to the triangle selected using the "Triangle" button. The backspace key can be used to erase errors. Once a word has been typed, click the blue "Enter" button to confirm your selection and close the window.

2.2.3 Selecting colors

The "Base Color" and "Surface Color" buttons open pull-down menus with an array of colors. Clicking on a color in either one of these menus causes the menu to disappear and the button to be displayed in its respective color. The "Base

Color" selection will determine the color of the $\mathbb{C}$-arc that forms the base of the selected triangle. Similarly, "Surface Color" will specify the color of the $\mathbb{R}$-arcs that comprise the surface of the triangle.

Once the user chooses a $\mathbb{C}$-arc, a cone point, a word, and two colors, he should left click on the blue "Enter" button in the menu bar. This tells the program to draw the specified triangle.

2.2.4 Selecting a coordinate system

To the right of the blue "Enter" button in the menu bar is a button labeled "Coordinates." The coordinates button brings up a pull down menu listing the available perspectives for viewing the triangles. These perspectives will be discussed in detail in a later section. Clicking on an item in this list will immediately redraw any triangles in the display using the new coordinates. In addition, all new triangles the user selects will be drawn in these coordinates.

2.2.5 Options

The rightmost button on the menu bar is labeled "Options." The options button opens a pull-down menu with three items: "Save", "Display Tiling", and "Hide Surfaces". "Save" opens a window allowing the user to choose a file and save a postscript picture of the display pane in that file. "Display tiling" will erase any currently drawn triangles and draw a section of the tiling. It also changes to a favorable coordinate system and hides the surfaces of the triangles in the tiling. Both of these changes can be undone after the tiling is drawn. "Hide Surfaces" is a toggle switch that allows the user to draw only the $\mathbb{C}$-arc bases of triangles, omitting the $\mathbb{R}$-arc surfaces. Switching this control will affect both the displayed

triangles and any new triangles that are selected.

2.2.6 Display

The display pane is the white rectangle directly underneath the menu bar, and its operation is fairly simple. All the triangles that have been selected are drawn simultaneously, in the display. Clicking the left mouse button inside the display will zoom in on the current location of the pointer. Similarly, the right button will zoom out. The middle button immediately saves the image in the display pane to a file titled temp.ps, overwriting whatever was there.

2.2.7 Changing drawn triangles

The log pane is beneath the display and shows what triangles the user has entered, and the tools to change them. The log consists of eighteen slots, each with an "erase" button, a "hide" button, and a white box that lists the details of the triangle in that slot. For each triangle, the listed details are the $\mathbb{C}$-circle, the cone point, the arc, the word applied to it and the selected colors. For example,

$I0S \to 102$ **012**

indicates that the slot is holding the triangle given by the short arc of I_0 coned to the fixed point of $I_1I_0I_2$, with the word $I_0I_1I_2$ applied to it. Note that the applied word appears in bold font to distinguish it from the cone point. To the right of the applied word, two vertical bands will appear representing the base color and the surface color for the triangle, from left to right.

The "erase" and "hide" buttons will affect the triangle whose details appear in the white box below them. Erase will remove the associated triangle from the display, and empty the white box below it. The next new triangle selected using

the menu bar will appear in this slot. The hide button will remove the associated triangle from the display, but keep it stored in memory and its slot occupied. The white box will turn gray and the hide button will now read "show." Clicking on show will restore the hidden triangle.

Also in the log pane is the red "Reset" button. Clicking on this button will erase the display completely, return the perspective to "flat 102", erase all of the slots, and generally return the program to the state of being originally launched. Hidden triangles are the exception to the reset command. These must be shown before they can be erased.

2.3 An Example Triangle

Recall that for the *short* arc of a $\mathbb{C}$-circle fixed by I_j and a flag associated to $I_k I_l I_m$, we denote the resulting triangle by $C\ \ short \to p_{jkl}$. In this section we will draw the triangle $\sigma(C_1\ \ short \to p_{102})$ using CHAT. We begin by left clicking on the "Triangle" button in the upper left corner of the window. When the new window has opened, we click on "I0 coned to 102" in the left hand column, followed by "short" in the right hand column. Left clicking on the blue "Enter" button in this window will finalize these choices and close the window. Next, we left click the "Word" button and type "3" The number three should appear in the window, and we can then click its "Enter" button to submit this word.

Clicking on the "Base Color" button in the menu bar opens a pull-down window. Move the pointer over the second square from the top, black, and left click to select this color. Following the same procedure for the "Surface Color" button, move the pointer over the second to last color, gray, and left click. Finally left click on the "Enter" button located on the menu bar. The resulting image

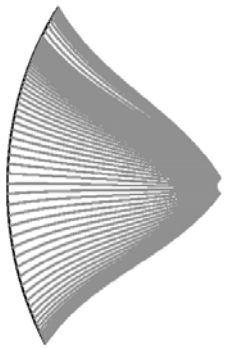

Figure 2.2: $\sigma(C_1 \ \ short \to p_{102})$

should be the same as figure 2.2.

We will use a shorthand for constructing images with CHAT, so that the reader may recreate the figures in this document. Each command will be on a separate line, and proceed in the left to right order of the menu bar. For example, I_0 to p_{102}, short

021

black

gray

would be the shorthand for drawing $I_0 I_2 I_1(C_0 \ \ short \to p_{102})$. The first line gives the commands to be entered in the "Base" window, followed by the command for the "Word" window, and lastly the base and surface colors respectively. If no entry for "Word" is necessary, the second line will display the character "-"

2.4 Drawing $\mathbb{C}$-arcs

There are two primary objects that CHAT draws: $\mathbb{C}$-arcs and $\mathbb{R}$-arcs. We begin by discussing the methods used to construct $\mathbb{C}$-arcs.

It is shown in [S0] that, given three distinct points in $\partial\mathbb{C}H^2$ not lying on a common $\mathbb{C}$-circle, they can be normalized to be of the form

$$(B(s), B(s)) \quad (B(s), B\bar{(}s)) \quad (B\bar{(}s), B\bar{(}s))$$

where

$$B(s) = \frac{s+i}{\sqrt{s+2s^2}} \qquad s \in [0, \infty]$$

The angular invariant of this triple of points will be $\pm \arctan s$, depending on the order taken. These three points may be used to define a representation ρ_s of the (∞, ∞, ∞) triangle group into $\mathbf{Isom}(\mathbb{C}H^2)$. The discrete, faithful representations correspond to $s \in [0, \sqrt{\frac{125}{3}}]$

The group of interest to us will be the image of the representation at the endpoint, $\sqrt{\frac{125}{3}}$. The triple of points will be

$$v_0 = (\beta, \beta) \quad v_1 = (\beta, \bar{\beta}) \quad v_2 = (\bar{\beta}, \bar{\beta}); \text{ where } \beta = \frac{i+\sqrt{\frac{125}{3}}}{\sqrt{2+\frac{250}{3}}}$$

The reader may verify that the angular invariant of these points is $\pm \arctan(\sqrt{\frac{125}{3}})$.

Let us now consider the $\mathbb{C}$-arc between v_i and v_j. We know that if we take a Heisenberg stereographic projection of $S^3 - \{v_i\}$ to $\mathcal{H}$ that sends v_j to (0,0), the $\mathbb{C}$-circle containing them will be sent to the t-axis in $\mathcal{H}$. This is because infinite $\mathbb{C}$-circles are mapped to vertical lines in $\mathcal{H}$ by such projections, and there is a unique $\mathbb{C}$-circle between v_i and v_j. The arcs of this circle will be given by the positive and negative parts of the t-axis.

This is the basis for the procedure in CHAT to create the $\mathbb{C}$-arcs between v_i and v_j in S^3. CHAT uses one Heisenberg stereographic projection, Ψ, from

$S^3 - \{(0,1)\}$ to $\mathcal{H}$, mapping $(1,0)$ to $(0,0)$. It also has a routine that takes two points, v_i and v_j, and outputs an element, M of $PU(2,1)$ that sends v_i to $(0,1)$ and v_j to $(1,0)$. The points on the $\mathbb{C}$-circle are given (in S^3) by $M^{-1}\Psi^{-1}((0,t))$ for $t \in [-\infty, \infty]$. The two arcs will then correspond to $t < 0$ and $t > 0$.

2.5 Drawing $\mathbb{R}$-arcs

The setup for drawing $\mathbb{R}$-circles is similar, but requires a bit more work. CHAT must take a point p on a $\mathbb{C}$-arc as well as a flag (E, q) and use the coning process to create the desired arc between p and q. Using the same routine as the previous section, CHAT finds an element A of $PU(2,1)$ that sends q to $(0,1)$ and another point on E to $(1,0)$. Letting Ψ is the Heisenberg stereographic projection of the previous section, we see that $\Psi \circ A$ will map E to the t-axis in $\mathcal{H}$. Now consider $\Psi(Ap) = (z_0, t_0)$ in $\mathcal{H}$. The $\mathbb{R}$-circle specified by the coning procedure intersects the t-axis at $(0, t_0)$. Then $o = A^{-1}\Psi((0,t_0))$ will be a third point in S^3 lying on the $\mathbb{R}$-circle we require. We then parametrize the $\mathbb{R}$-arc, ξ, with parameter $s \in [0,1]$ by:

$$\tilde{\xi_s}(p,q,o) = (1-s)\tilde{p} + s\tilde{q} + s(s-1)\tilde{o}$$

where the lifts $\tilde{p}, \tilde{q}, \tilde{o}$ are chosen so that

$$\langle \tilde{p}, \tilde{q} \rangle = \langle \tilde{q}, \tilde{o} \rangle = \langle \tilde{o}, \tilde{p} \rangle = r \in \mathbb{R}$$

Claim 2.5.1 *the projection of $\tilde{\xi_s}$ to $\partial\mathbb{C}H^2$ parameterizes the $\mathbb{R}$-arc through p and*

q that omits o

Proof: A quick computation shows that

$$\langle \tilde{\xi}_s, \tilde{\xi}_s \rangle = 2r(s(1-s) + (1-s)(s^2-s) + s(s^2-s)) = 2r(0)$$

and therefore that every point on the parameterization is in N_0. By choosing the lifts to have pairwise real inner products, we know by properties of $\langle , \rangle$ that the triple product

$$\langle \tilde{\xi}_s, \tilde{\xi}_t \rangle \langle \tilde{\xi}_t, \tilde{\xi}_n \rangle \langle \tilde{\xi}_n, \tilde{\xi}_s \rangle$$

will always be real for distinct $s, t, n \in [0, 1]$. This means that any three distinct points on $\tilde{\xi}_s$ will satisfy the angular invariant for points on an $\mathbb{R}$-circle. $\square$

2.6 Perspectives

In the menu labeled "coordinates" in CHAT is a list of six different options for viewing the triangles. These options have three flavors. The first three items are all flat, and the next three are labeled "cyl," short for cylindrical. A variety of projections is helpful in determining the intersection behavior of triangles. This is the most frequent use of CHAT and, as these triangles naturally exist in $\partial \mathbb{C}H^2$, many two dimensional images result in a loss of information. Two triangles that appear to intersect in one perspective may be disjoint in another. In addition, viewing several perspectives can help the user build an idea of how the triangles sit in $\partial \mathbb{C}H^2$.

The flat and the cylindrical coordinates are both obtained by using stereo-

graphic projection to map $\partial\mathbb{C}H^2$ to $\mathcal{H}$. As a result, they both involve a choice of a point to leave out, the infinite point in $\mathcal{H}$. They involve other choices as well, but the resulting views are so similar that only the infinite point matters. This choice is reflected in the coordinates menu by the initial part of the label. For example, "Fix(102) flat" takes the triangle from $\partial\mathbb{C}H^2$ to $\mathcal{H}$, mapping the fixed point of $I_1I_0I_2$ to ∞ in $\mathcal{H}$. The flat and cylindrical maps then go a step further.

	$\mathbb{C}$	$S^1 \times \mathbb{R}$
p_{102}	p102 Flat	p102 Cyl
p_{012}	p012 Flat	p012 Cyl
p_{021}	p021 Flat	p021 Cyl

Table 2.1: A perspective chart of infinite points against range

Table 2.1 lists the six coordinate systems available in CHAT. The top row gives the ranges of the coordinates, while the left column lists the possible points mapped to infinity in $\mathcal{H}$. Each entry in the table lists a coordinate chart as it appears in CHAT.

2.6.1 Flat

Given a collection of points in $\mathcal{H}$, the flat projection simply forgets the second coordinate, t. Equivalently, it projects all the points onto the set $\mathbb{C} \times 0$. In this perspective, all $\mathbb{C}$-circles that do not go through infinity appear as round circles. In contrast, finite $\mathbb{R}$-circles appear as lemniscates. Infinite $\mathbb{R}$-circles appear as straight lines and infinite $\mathbb{C}$-circles are simply dots. See [Go] for more details. The flat views are typically most revealing for triangles that have a common cone

point.

2.6.2 Cylindrical

Slightly more sophisticated is the cylindrical projection. This projection leaves the t coordinate unaffected, but takes the z coordinate to its unit circle representative, i.e., takes $re^{i\theta}$ to $e^{i\theta}$. This is equivalent to projecting points in $\mathcal{H}$ to the unit cylinder about the t-axis. We then unwrap the cylinder, giving us a two dimensional image. In this perspective, infinite $\mathbb{R}$-circles intersecting the t-axis appear as dots because they are straight lines with constant t-value. Finite $\mathbb{C}$-circles that link the t-axis, on the other hand, become smooth periodic curves. This is due to the fact that a finite $\mathbb{C}$-circle in $\mathcal{H}$ is an ellipse. When viewing images in cylindrical coordinates, it is important to remember that the image is cut in the process of unwrapping the cylinder, so a sufficiently wide zoom should be imagined glued along the vertical edges. This perspective is frequently helpful for looking at triangles whose bases share a common point.

Chapter 3

Empirical Evidence

In this section we present visual evidence from CHAT to support our main conjecture.

Conjecture 3.1 *There exists a tiling of* Ω*, the domain of discontinuity for* Γ*, by embedded octahedra. The faces of these octahedra are triangles constructed from* $\mathbb{C}$*- and* $\mathbb{R}$*-arcs.*

We will proceed to give evidence that a specific octahedron is embedded and that this octahedron generates the tiling. Throughout this chapter, we will say that a figure "shows" or "establishes" a result. We do not mean that these figures constitute a rigorous proof, only that the figure provides evidence that the result may be true.

3.1 Defining an Octahedron in the tiling

We begin by describing an octahedron as a quadrilateral coned to two points. Recall that for a point on a $\mathbb{C}$-arc and we may use the flag for an element of

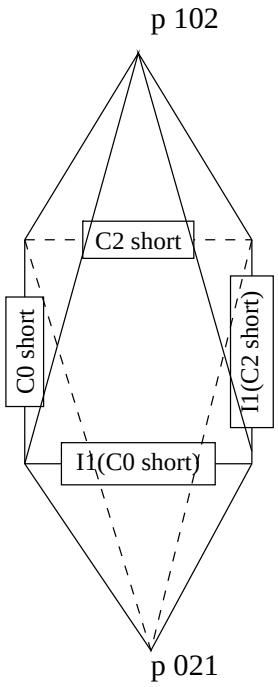

Figure 3.1: A schematic for an octahedron in the tiling

the group to apply the coning procedure. The edges of the quadrilateral are all $\mathbb{C}$-arcs, and the each point we cone to is an element of a flag. We may then connect each edge of the quadrilateral to these points by $\mathbb{R}$-arcs via the coning procedure. As before, labeling the $\mathbb{C}$-arcs I_j fixes by $C_j\ short$ and $C_j\ long$, our specific example starts with the $\mathbb{C}$-arcs:

$C_0\ short,\ I_1(C_0\ short),\ C_2\ short,\ and\ I_1(C_2\ short)$

These arcs make up the quadrilateral for our octahedron. The two cone points are the fixed point of $I_1I_0I_2$ and the fixed point of $I_0I_2I_1$. Figure 3.1 illustrates this construction schematically on a Euclidean octahedron.

We came to this octahedron by analyzing a set of triangles, specifically the set generated by taking each $\mathbb{C}$-arc and coning it to four fixed points. One fixed point came from the structures defined in [S0]. Another came from mapping a different

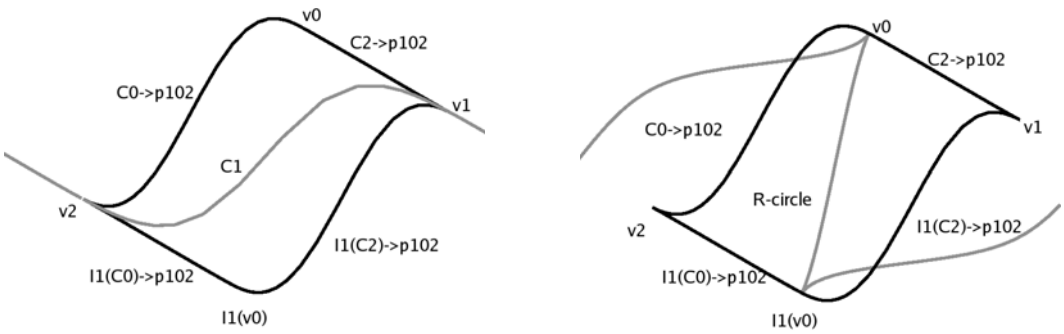

(a) **(b)**

Figure 3.2: The quadrilateral with its symmetric $\mathbb{R}$-circle and $\mathbb{C}$-circle

flag to the t-axis in $\mathcal{H}$. When viewing all the $\mathbb{C}$-arcs in cylindrical coordinates under this map, the same $\mathbb{C}$-arc appears in a quadrilateral tiling. The remaining two fixed points were determined by reflecting in the $\mathbb{C}$-arc.

The fact that these are all short arcs is not coincidental. While the long arcs do arrange themselves in a pattern as well, they do not result in an octahedral tiling. As no *long* arcs appear in this or any other octahedron in our tiling, we assume all $\mathbb{C}$-arcs to be *short* for the duration of the section and omit the labels. For simplicity of notation, we will label the six projections from Heisenberg space that CHAT uses, and refer to them by number.

Projection I $\equiv p_{102} \mapsto \infty$, $(z,t) \mapsto z$

Projection II $\equiv p_{012} \mapsto \infty$, $(z,t) \mapsto z$

Projection III $\equiv p_{021} \mapsto \infty$, $(z,t) \mapsto z$

Projection IV $\equiv p_{102} \mapsto \infty$, $(z,t) \mapsto (arg(z),t)$

Projection V $\equiv p_{012} \mapsto \infty$, $(z,t) \mapsto (arg(z),t)$

Projection VI $\equiv p_{021} \mapsto \infty$, $(z,t) \mapsto (arg(z),t)$

3.2 Symmetries of the Octahedron

Our octahedron has two natural symmetries we wish to take advantage of. Note that the $\mathbb{C}$-circle C_1 does not appear in the $\mathbb{C}$-arc quadrilateral of our octahedron. Instead, it bisects the quadrilateral, intersecting it at exactly two vertices, as shown in Figure 3.2 (a) with the quadrilateral in black and C_1 in gray. This picture is in cylindrical coordinates, so the left edge of the image is actually glued to the right edge, thus completing the gray circle. The cone point p_{102} is mapped to infinity in this picture. Reflection in C_1 sends this quadrilateral to itself and swaps p_{102} with p_{021}.

Given an $\mathbb{R}$-circle, R, there is a unique inversion, O, in $\mathbf{I}\text{som}(\mathbb{C}H^2)$. This inversion has R as its fixed point set and has order 2. It is also anti-holomorphic, having the form $O((z,w)) = P(\bar{z},\bar{w})$ with $P \in PU(2,1)$

The second symmetry is an isometry of this form. There is a $\mathbb{R}$-circle which intersects the quadrilateral at the vertices missed by C_1. The inversion in this circle is the other symmetry of our octahedron, and we will refer to it as the $\mathbb{R}$-reflection. Figure 3.2 (b) shows the $\mathbb{R}$-circle in gray and the quadrilateral in black, with p_{102} mapped to infinity. This symmetry also swaps the cone points of the octahedron, but swaps the vertices of the quadrilateral fixed by C_1. Although not clear in the figure, the $\mathbb{R}$-circle intersects the quadrilateral only at its vertices. We list the actions of both symmetries below.

The $\mathbf{I_1}$ action

$\mathbf{C_0} \to \mathbf{p_{102}} \longmapsto I_1(C_0) \to p_{021}$

$\mathbf{I_1(C_0)} \to \mathbf{p_{102}} \longmapsto C_0 \to p_{021}$

$\mathbf{C_0} \to \mathbf{p_{021}} \longmapsto I_1(C_0) \to p_{102}$

The $\mathbb{R}$-reflection action

$\mathbf{C_0} \to \mathbf{p_{102}} \longmapsto C_2 \to p_{021}$

$\mathbf{I_1(C_0)} \to \mathbf{p_{102}} \longmapsto I_1(C_2) \to p_{021}$

$\mathbf{C_0} \to \mathbf{p_{021}} \longmapsto C_2 \to p_{102}$

$\mathbf{I_1(C_0)} \to \mathbf{p_{021}} \longmapsto C_0 \to p_{102}$ $\quad$ $\mathbf{I_1(C_0)} \to \mathbf{p_{021}} \longmapsto I_1(C_2) \to p_{102}$

$\mathbf{C_2} \to \mathbf{p_{102}} \longmapsto I_1(C_2) \to p_{021}$ $\quad$ $\mathbf{C_2} \to \mathbf{p_{102}} \longmapsto C_0 \to p_{021}$

$\mathbf{I_1(C_2)} \to \mathbf{p_{102}} \longmapsto C_2 \to p_{021}$ $\quad$ $\mathbf{I_1(C_2)} \to \mathbf{p_{102}} \longmapsto I_1(C_0) \to p_{021}$

$\mathbf{C_2} \to \mathbf{p_{021}} \longmapsto I_1(C_2) \to p_{102}$ $\quad$ $\mathbf{C_2} \to \mathbf{p_{021}} \longmapsto C_0 \to p_{102}$

$\mathbf{I_1(C_2)} \to \mathbf{p_{021}} \longmapsto C_2 \to p_{102}$ $\quad$ $\mathbf{I_1(C_2)} \to \mathbf{p_{021}} \longmapsto I_1(C_0) \to p_{102}$

Three facts about these symmetries help to distinguish their actions

- They both transpose cone points
- I_1 transposes itself with the identity
- $\mathbb{R}$-reflection transposes C_0 with C_2 in the notation for each triangle

3.3 Showing the octahedron is embedded

In order to provide evidence that the octahedron is embedded we take pairs of faces and show they have disjoint interiors. There are 28 such pairings for an octahedron. Using the two symmetries discussed above and their product, we can simplify this to ten inequivalent pairs. Because each symmetry will fix four pairs, we have four equivalence classes with four pairs and six equivalence classes with two pairs. These cases are analyzed in seven subsections. Below we list all 28 pairs, grouped by the subsection dealing with those pairs. The representatives which each subsection analyzes in detail are listed in bold.

3.3.1: Opposite Faces

$\mathbf{C_0 \to p_{102}}$ **and** $\mathbf{I_1(C_2) \to p_{021}}$

$C_2 \to p_{102}$ and $I_1(C_0) \to p_{021}$

3.3.2: Common $\mathbb{C}$-arc

$\mathbf{C_0 \to p_{102}}$ **and** $\mathbf{I_1(C_2) \to p_{021}}$

$C_2 \to p_{102}$ and $I_1(C_0) \to p_{021}$

$C_2 \to p_{021}$ and $I_1(C_0) \to p_{102}$

$C_0 \to p_{021}$ and $I_1(C_2) \to p_{102}$

$C_2 \to p_{021}$ and $I_1(C_0) \to p_{102}$

$C_0 \to p_{021}$ and $I_1(C_2) \to p_{102}$

3.3.3: Common $\mathbb{R}$-arc and $\mathbf{I_1}$

$\mathbf{C_0 \to p_{102}}$ **and** $\mathbf{C_0 \to p_{021}}$

$I_1(C_0) \to p_{021}$ and $I_1(C_0) \to p_{102}$

$C_2 \to p_{021}$ and $C_2 \to p_{102}$

$I_1(C_2) \to p_{102}$ and $I_1(C_2) \to p_{021}$

3.3.4: Common $\mathbb{R}$-arc and $\mathbb{R}$-ref.

$\mathbf{C_0 \to p_{102}}$ **and** $\mathbf{I_1(C_0) \to p_{102}}$

$I_1(C_0) \to p_{021}$ and $C_0 \to p_{021}$

$C_2 \to p_{021}$ and $I_1(C_2) \to p_{021}$

$I_1(C_2) \to p_{102}$ and $C_2 \to p_{102}$

3.3.5: Pairs Fixed by Compos.

$\mathbf{C_0 \to p_{102}}$ **and** $\mathbf{I_1(C_2) \to p_{102}}$

$I_1(C_0) \to p_{021}$ and $C_2 \to p_{021}$

$\mathbf{C_0 \to p_{021}}$ **and** $\mathbf{I_1(C_2) \to p_{021}}$

$I_1(C_0) \to p_{102}$ and $C_2 \to p_{102}$

3.3.6: Pairs fixed by $\mathbf{I_1}$

$\mathbf{C_0 \to p_{021}}$ **and** $\mathbf{I_1(C_0) \to p_{102}}$

$C_2 \to p_{102}$ and $I_1(C_2) \to p_{021}$

$\mathbf{C_0 \to p_{102}}$ **and** $\mathbf{I_1(C_0) \to p_{021}}$

$C_2 \to p_{021}$ and $I_1(C_2) \to p_{102}$

3.3.7: Pairs Fixed by $\mathbb{R}$-reflection

$\mathbf{C_0 \to p_{102}}$ **and** $\mathbf{C_2 \to p_{021}}$

$I_1(C_0) \to p_{021}$ and $I_1(C_2) \to p_{102}$

$\mathbf{C_0 \to p_{021}}$ **and** $\mathbf{C_2 \to p_{102}}$

$I_1(C_0) \to p_{102}$ and $I_1(C_2) \to p_{021}$

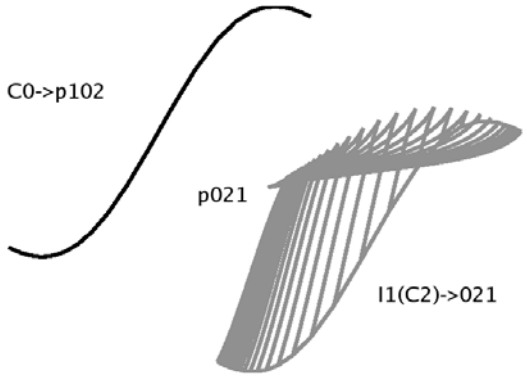

Figure 3.3: $C_0 \to p_{102}$ and $I_1(C_2) \to p_{021}$

3.3.1 Opposite Faces

There are four pairs of opposite faces on an octahedron, and they are all equivalent to the pair

$C_0 \to p_{102}$ and $I_1(C_2) \to p_{021}$

by symmetry. Figure 3.3 shows this pair in Projection IV. C_0 is drawn in black, and $I_1(C_2) \to p_{021}$ is drawn in gray. Note that we do not see the surface of $C_0 \to p_{102}$ because this projection maps p_{102} to infinity, hence the $\mathbb{R}$-arcs of the surface are perpendicular to the plane of the image. We see that these two triangles are completely disjoint.

3.3.2 A Common $\mathbb{C}$-arc

We have four pairs of faces that intersect along a $\mathbb{C}$-arc of the quadrilateral, represented by the pair

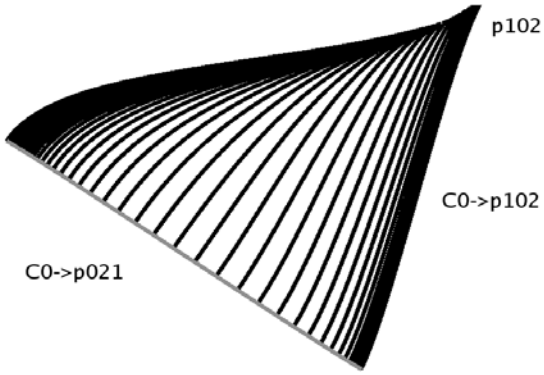

Figure 3.4: $C_0 \to p_{102}$ and $C_0 \to p_{021}$

$C_0 \to p_{102}$ and $C_0 \to p_{021}$

Figure 3.4 shows this pair in Projection VI. $C_0 \to p_{102}$ is drawn in black, while $C_0 \to p_{021}$ is drawn in gray. As before, the surface arcs of the gray triangle are straight lines perpendicular to the page in this perspective, since the cone point p_{021} is mapped to infinity. By definition, these triangles intersect along the $\mathbb{C}$-arc C_0. The image allows us to see that all the black arcs are monotonically increasing in the t coordinate, up to p_{102}, hence they do not intersect the surface of the gray triangle other than their common endpoints.

3.3.3 A Common $\mathbb{R}$-arc and I_1

The next class of pairs is characterized by intersecting along an $\mathbb{R}$-arc and sharing a vertex fixed by I_1. We choose

$C_0 \to p_{102}$ and $I_1(C_0) \to p_{102}$

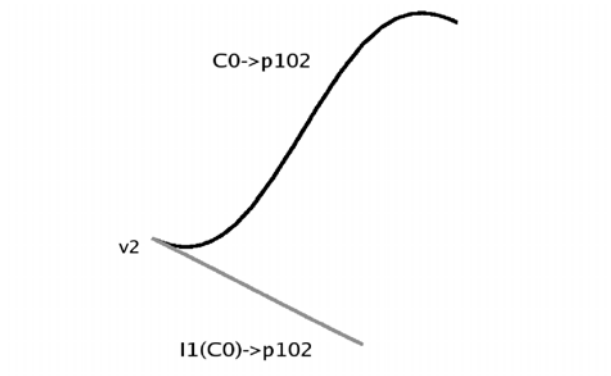

Figure 3.5: $C_0 \to p_{102}$ and $I_1(C_0) \to p_{102}$

as a representative, shown in Figure 3.5 using Projection IV. $C_0 \to p_{102}$ is drawn in black and the other triangle is drawn in gray. In this case, both triangles share a cone point, p_{102} that is mapped to infinity, so neither surface is drawn. This picture highlights the fact that the two triangles also share an endpoint of their respective bases, v_2. Accordingly, we can conclude that the two triangles have a common $\mathbb{R}$-arc from v_2 to p_{102}, but all the other arcs meet only at infinity.

3.3.4 A Common $\mathbb{R}$-arc and $\mathbb{R}$-reflection

The final equivalence class of cardinality four contains pairs of faces intersecting along an $\mathbb{R}$-arc with an endpoint fixed by reflection in the $\mathbb{R}$-circle. The representative is the pair

$$C_0 \to p_{102} \text{ and } C_2 \to p_{102}$$

Figure 3.6 displays this pair in Projection IV, with $C_0 \to p_{102}$ drawn in black. As in the last class, no $\mathbb{R}$-arcs are shown because the common cone point is mapped

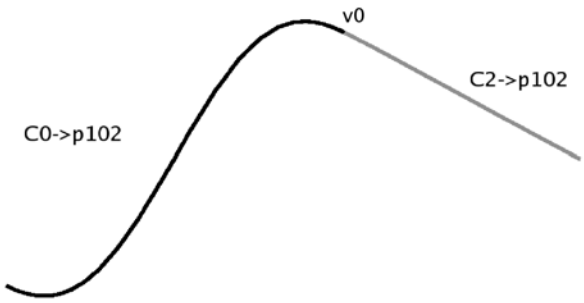

Figure 3.6: $C_0 \to p_{102}$ and $C_2 \to p_{102}$

to infinity. As a result, all the $\mathbb{R}$-arcs are lines perpendicular to the plane of the page. The fact that the $\mathbb{C}$-arcs do not overlap suggests that the two faces have no interior intersections. The two triangles share the vertex v_0, which is fixed by reflection in the $\mathbb{R}$-circle, and thus they share an $\mathbb{R}$-arc from v_0 to p_{102}. The two $\mathbb{C}$-arcs diverge away from v_0, so their common $\mathbb{R}$-arc and p_{102} are the only intersections of these two triangles.

3.3.5 Pairs Fixed by the Composition

There are four pairs fixed by the composition of the $\mathbb{R}$-reflection with I_1. These four pairs are divided into two equivalence classes, each of order two. As a representative for the first class, we take

$$C_0 \to p_{102} \text{ and } I_1(C_2) \to p_{102}$$

This pair is shown in Figure 3.7 (a) using Projection IV. $C_0 \to p_{102}$ is in black, while $I_1(C_2) \to p_{102}$ is drawn in gray. We can see immediately from this image

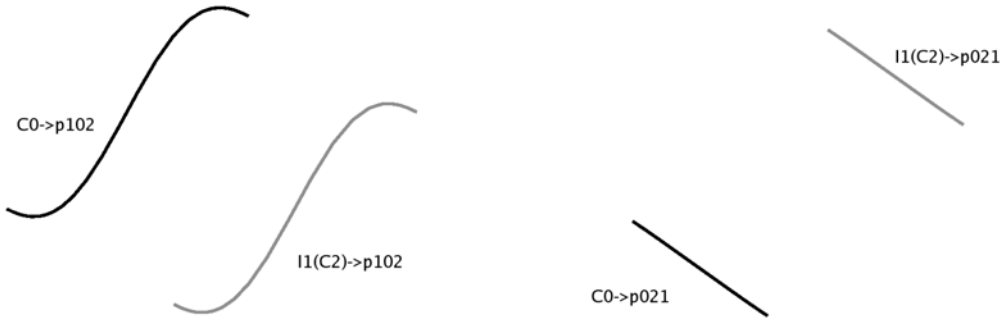

(a) **(b)**

Figure 3.7: Pairs fixed by the product of the two reflections

that the two $\mathbb{C}$-arcs are completely disjoint. As they share the cone point p_{102} which is mapped to infinity, we know that the unique intersection of these surfaces is that point.

Figure 3.7 (b) displays a representative for the other class fixed by this symmetry in Projection VI. Similarly to 3.7 (a), the two $\mathbb{C}$-arcs are obviously disjoint and we may conclude again that the two triangles intersect only at their common cone point, p_{021}. The representative for this class is

$$C_0 \to p_{021} \text{ and } I_1(C_2) \to p_{021}$$

3.3.6 Pairs fixed by I_1

The equivalence classes fixed under reflection in C_1 are slightly more difficult to see. We begin with Figures 3.8 (a) and (b), which is the easier case of the pair

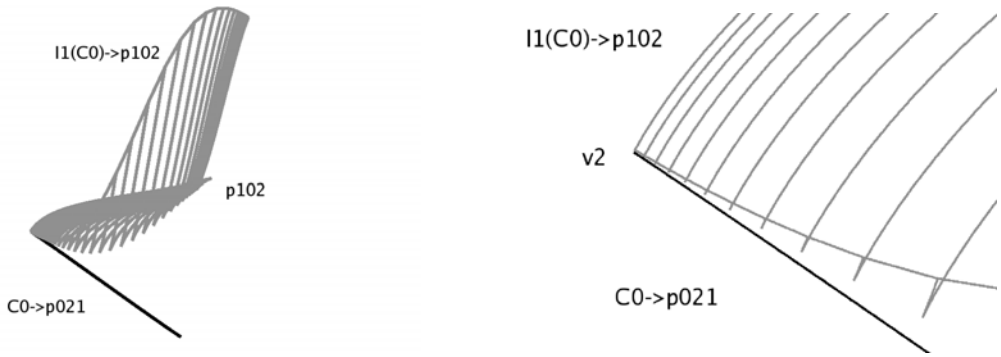

(a) **(b)**

Figure 3.8: $C_0 \to p_{021}$ and $I1(C_0) \to p_{102}$ (a) and a closer view near v_2 (b)

$C_0 \to p_{021}$ and $I_1(C_0) \to p_{102}$

These pictures are in Projection VI, with $C_0 \to p_{021}$ pictured in black. Figure 3.8 (a) gives an overall view of the two triangles. We can see that the region of concern is near their common vertex, v_2. It is clear that the $\mathbb{C}$-arcs diverge away from this point, but the behavior of the $\mathbb{R}$-arcs is less certain. Figure 3.8 (b) gives a close-up of the region near v_2, from which we can see that the gray $\mathbb{R}$-arcs remain disjoint from the black $\mathbb{C}$-arc. Because the surface of the black triangle is perpendicular to the image, we may conclude that the only intersection of these triangles is v_2.

A greater challenge is posed by the second equivalence class, as no single image yields the desired result. Figure 3.9 (a) and (b) show two perspectives of the same pair

$C_0 \to p_{102}$ and $I_1(C_0) \to p_{021}$

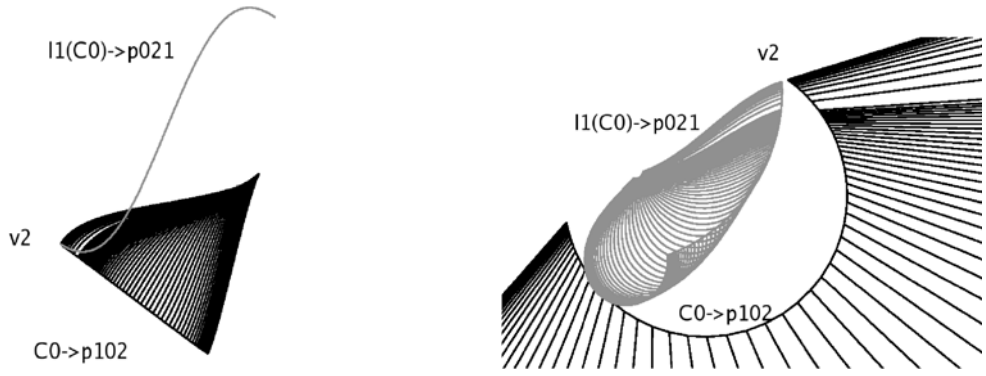

(a) **(b)**

Figure 3.9: Two perspectives of $C_0 \to p_{102}$ and $I_1(C_0) \to p_{021}$

Figure 3.9 (a) shows that the two triangles are disjoint sufficiently far away from their common vertex v_2, using Projection VI. $C_0 \to p_{102}$ is drawn in black while the other triangle is in gray. The region that requires further analysis is near v_2. This image makes it seem as though the interiors of the surface intersect in this region. Fortunately this is not the case.

Figure 3.9 (b) is drawn with Projection I. It shows that the questionable region is in fact not an interior intersection. The two triangles are converging to the point v_2, but they remain disjoint aside from this point. It would appear that there is another possible intersection on the other end of the gray $\mathbb{C}$-arc, but we were able to establish otherwise with Figure 3.9 (a). Together, these images show that the pair is disjoint, save v_2.

The reader may observe that the surface $\mathbb{R}$-arcs are not uniformly spaced along the $\mathbb{C}$-arcs in Figure 3.9. To resolve detail near the endpoints of the $\mathbb{C}$-arc and detail along the rest of the arc, CHAT changes the way it samples points along the arc. This phenomenon will reappear in figures throughout the chapter.

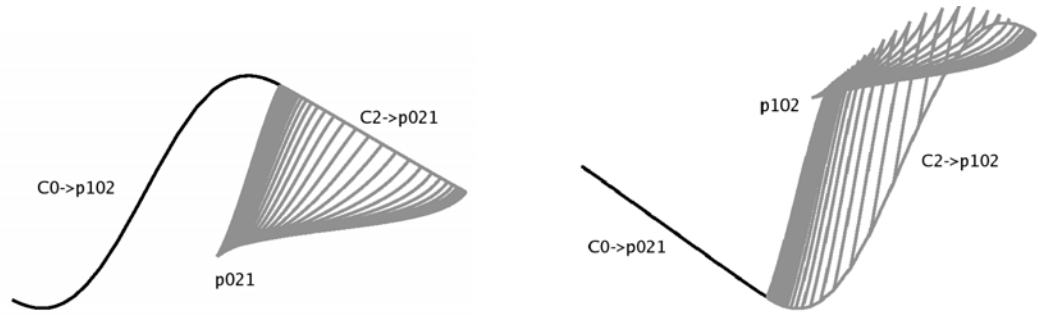

(a) **(b)**

Figure 3.10: Pairs fixed by the $\mathbb{R}$ reflection

3.3.7 Pairs Fixed by $\mathbb{R}$-reflection

The last two equivalence classes are pairs fixed by reflection in the symmetric $\mathbb{R}$-circle. The representatives are

$C_0 \to p_{102}$ and $C_2 \to p_{021}$ Figure 3.10 (a)

$C_0 \to p_{021}$ and $C_2 \to p_{102}$ Figure 3.10 (b)

Figure 3.10 (a) is in Projection IV, while 3.10 (b) is in Projection VI. 3.10 (a) shows $C_0 \to p_{102}$ in black, but again its surface is not drawn since p_{102} is mapped to infinity. Accordingly, the $\mathbb{R}$-arcs of the surface are lines perpendicular to the plane containing the figure. We can see that the gray arcs stay well away from the black $\mathbb{C}$-arc, except for their common point v_0. As no $\mathbb{R}$-arcs overlap the black $\mathbb{C}$-arc, we may conclude that v_0 is their only intersection.

Figure 3.10 (b) has $C_0 \to p_{021}$ drawn in black. Again, its cone point is mapped to infinity, so we see only the gray surface. These two triangles share the same

vertex, v_0, as the previous two. We see that the gray $\mathbb{R}$-arcs remain disjoint from the black arc away from this point. As there is no part of the gray surface overlapping the black arc, we conclude that v_0 is the only intersection of these surfaces.

3.4 Generating the Tiling

Having provided evidence that the octahedron is indeed embedded, we produce the tiling by taking the orbit of this octahedron under the group Γ. We will provide images from CHAT that support the conjecture that the octahedra in the orbit are pairwise disjoint, i.e. that we have a bona-fide tiling. From [S0] we know there are three special topological spheres with disjoint interiors in $\partial\mathbb{C}H^2$. The group action of Γ moves these spheres around the domain of discontinuity while preserving this relation. We claim that each of our octahedra is divided into two parts by one of these spheres. Moreover, each face in the 2-skeleton of an octahedron intersects its dividing sphere along an $\mathbb{R}$-arc. Employing the symmetries of our octahedra mentioned above, it will suffice to show that two of the triangular faces of our selected octahedra each intersect a specific sphere along an $\mathbb{R}$-arc, and that, aside from this intersection, the faces are outside the sphere. In addition, we must show the same two triangles do not intersect the interiors of the remaining two spheres

The three special spheres are simple to describe. We simply take one of our three generating $\mathbb{C}$-circles, C_j, and cone it to the fixed points of $I_jI_{j-1}I_{j+1}$ and $I_jI_{j+1}I_{j-1}$ using the same coning process as the octahedron. The specific sphere that divides our chosen octahedron is C_1 coned to p_{102} and p_{120}. Note that $p_{120} = p_{021}$ since their corresponding elements are inverses. We will denote this

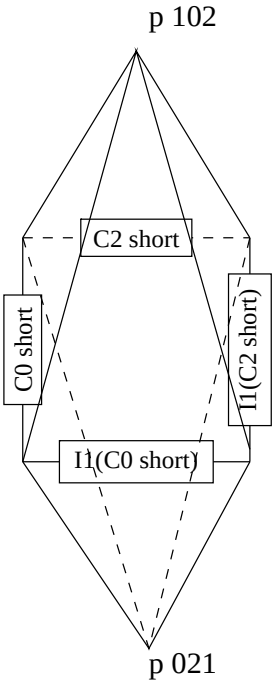

Figure 3.11: A schematic for an octahedron in the tiling

sphere by S_1, and in general denote the sphere of C_j by S_j. We will write "the p_{klm} half of S_j" to mean the portion of S_j given by coning C_j to p_{klm}. We will use the two triangles $C_0 \to p_{102}$ and $C_2 \to p_{102}$ as representative faces of our specific octahedron.

We reprint the schematic of the octahedron in Figure 3.11 for the convenience of the reader.

3.5 The Dividing Sphere

Let S_1° denote the three dimensional topological ball that S_1 bounds in $\partial\mathbb{C}H^2$. We wish to support the claim that four faces of our octahedron are contained in $S_1 \cup S_1^\circ$ and the remaining four are contained in $\partial\mathbb{C}H^2 - \{S_1^\circ\}$. Consider the following lemma

Lemma 3.5.1. *Suppose we have the following information about the intersections of* $C_0 \to p_{102}$ *and* $C_2 \to p_{102}$ *with* S_1

- $(C_0 \to p_{102}) \cap S_1$ *contains an* $\mathbb{R}$*-arc,* R_1*, joining* v_2 *and* p_{102}*.*
- $(C_2 \to p_{102}) \cap S_1$ *contains an* $\mathbb{R}$*-arc,* R_2*, joining* v_1 *and* p_{102}*.*
- $(C_0 \to p_{102}) - \{R_1\}$ *and* $(C_2 \to p_{102}) - \{R_2\}$ *are disjoint from the* p_{102} *half of* S_1*.*
- $(C_0 \to p_{102}) - \{R_1\}$ *and* $(C_2 \to p_{102}) - \{R_2\}$ *are disjoint from the* p_{021} *half of* S_1
- $C_0 \to p_{102}$ *and* $C_2 \to p_{102}$ *are disjoint from* S_1°

Then four faces of our octahedron are contained in $S_1 \cup S_1^\circ$ *and the remaining four faces are contained in* $\partial\mathbb{C}H^2 - \{S_1^\circ\}$*.*

Proof. The suppositions of the lemma establish that $C_0 \to p_{102}$ and $C_2 \to p_{102}$ are contained in $\partial\mathbb{C}H^2 - \{S_1^\circ\}$. The $\mathbb{R}$-reflection symmetry of the octahedron will map these faces to $C_2 \to p_{021}$ and $C_0 \to p_{021}$ and stabilize $S_1 \cup S_1^\circ$. This proves the second conclusion of the lemma. To show that the other four faces are contained in $S_1 \cup S_1^\circ$, we need only note that the map I_1 stabilizes S_1 and maps S_1° to $\partial\mathbb{C}H^2 - \{S_1^\circ \cup S_1\}$. Since I_1 is a symmetry of our octahedron, it maps these four faces contained in $\partial\mathbb{C}H^2 - \{S_1^\circ\}$ to the remaining four faces, which must then lie in $S_1 \cup S_1^\circ$. □

The first two suppositions of the lemma follow from the definitions of our objects. Note that v_2 is an endpoint of C_0 *short*, hence a vertex of $C_0 \to p_{102}$. Similarly, v_1 is a vertex of $C_2 \to p_{102}$. Both v_1 and v_2 lie on C_1 and are coned

to p_{102} in S_1. It follows that the faces intersect S_1 along the arcs $v_1 \to p_{102}$ and $v_2 \to p_{102}$, as desired. We handle the remaining suppositions in subsections

3.5.1 The p_{102} half

We have already shown the visual evidence supporting the third supposition of the lemma. Recall that Figure 3.2 (a) adequately shows that the two triangles do not additionally intersect the p_{102} half of S_1. In this image p_{102} is mapped to infinity and all the $\mathbb{R}$-arcs are straight lines perpendicular to the page. Since the $\mathbb{C}$-arcs of the image do not overlap, the figure demonstrates the third supposition of the lemma.

3.5.2 The p_{021} half

The fourth supposition of the lemma involves the intersection of the triangles with the p_{021} half of S_1. We will break the p_{021} half of S_1 into two triangles, $C_1\ long \to p_{021}$ and $C_1\ short \to p_{021}$, defined by separating the two arcs of C_1 at v_1 and v_2. We will treat our two faces in separate sets of images.

Figures 3.12 (a) and (b) both utilize Projection III. In 3.12 (a) we see the face $C_0\ short \to p_{102}$ in black, and the triangle $C_1 long \to p_{021}$ of S_1 in gray. The surface of the gray triangle has a vertex at infinity in this projection, so the norms of its constituent $\mathbb{R}$-arcs are monotonically increasing. The black surface, in contrast, is finite and its interior is separated from that of the gray triangle.

Figure 3.12 (b) is quite similar,using the same projection and color scheme, but displaying the triangle $C_1\ short \to p_{021}$ instead. Again, the image makes it clear that the interiors of the surfaces are disjoint. These two pictures, along with the earlier discussion of the p_{102} half of S_1. complete our understanding of

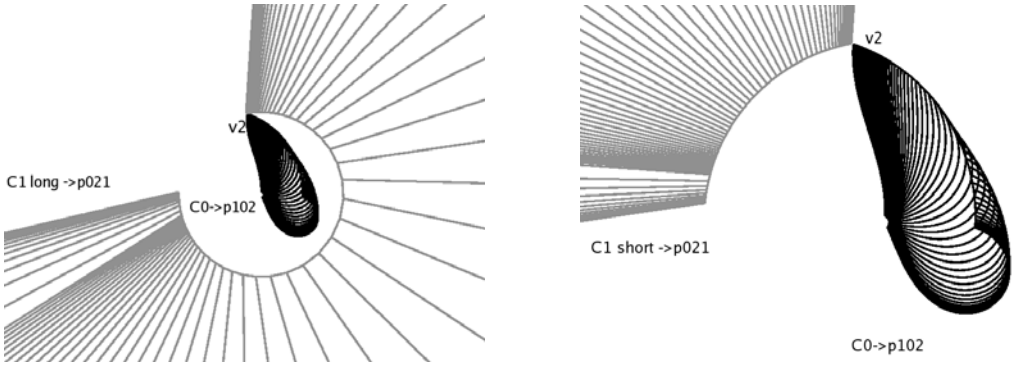

(a) **(b)**

Figure 3.12: $C_0 \to p_{102}$ with long (a) and short triangles (b) from the p_{021} half of S_1

the intersection of our face $C_0 \to p_{102}$ with S_1

Next we discuss the intersection of our face $C_2 \to p_{102}$ with the p_{021} half of S_1. As before, we break up this half of S_1 into $C_1 \ \ long \to p_{021}$ and $C_1 \ \ short \to p_{021}$ and analyze them separately.

Figures 3.13 (a) and (b) are both in Projection IV with the face of our octahedron in black, and the triangle from S_1 in gray. Figure 3.13 (a) gives an overall idea of how the two triangles intersect. The surface arcs of the black triangle are coned to infinity in 3.13 and thus not shown. We can see that the black arc is noticeably distinct from the gray surface away from the vertex v_1. Figure 3.13 (b) displays a closer view of the area near v_1. The gray surface converges to the black arc, but never crosses it. From this we determine that the surface interiors do not intersect.

We see the remaining triangle, $C_1 \ \ short \to p_{102}$, in gray in Figures 3.14 (a) and (b). These figures are in Projection VI, so the gray surface is not shown. Figure 3.14 (a) provides reasonably convincing evidence that the two triangles

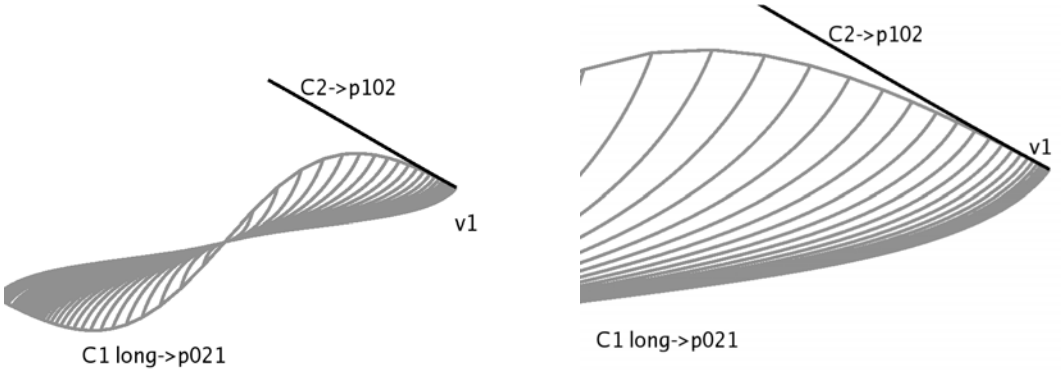

(a) **(b)**

Figure 3.13: $C_2 \to p_{102}$ with the long triangle from the p_{021} half of S_1 (a) and the region near v_1 (b)

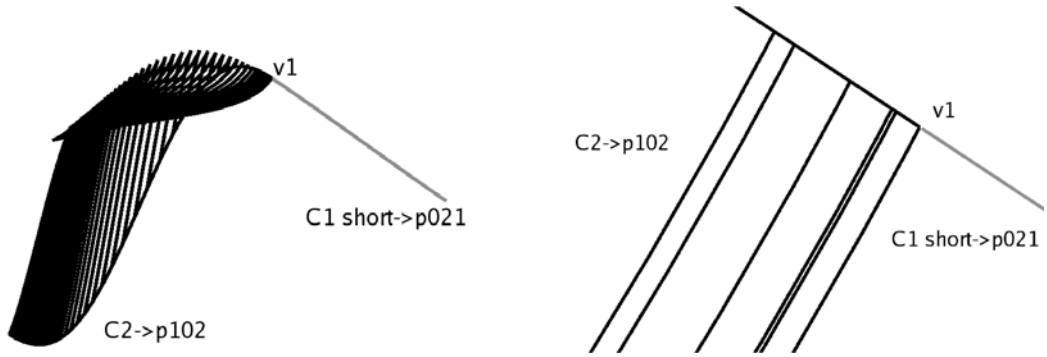

(a) **(b)**

Figure 3.14: $C_2 \to p_{102}$ with the short triangle from the p_{021} half of S_1 (a) and the region near v_1 (b)

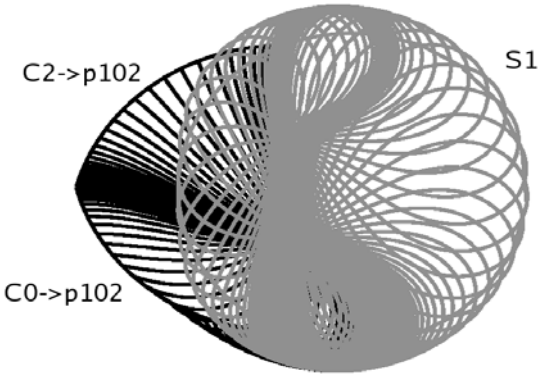

Figure 3.15: The sphere S_1 in gray with the two triangles in black

have disjoint interiors, as the black surface always remains on the left side of the gray arc. We also give Figure 3.14 (b) to show the region near v_1 in greater detail, which makes it clear that the black surface interior never touches the gray arc. This picture concludes the analysis of the intersection of $C_2 \to p_{102}$ with S_1.

3.5.3 Disjointness from S_1°

Finally, we must support the fifth supposition of Lemma 3.5.1 that these two faces of our octahedron, $C_0 \to p_{102}$ and $C_2 \to p_{102}$, are outside of S_1. Demonstrating the claim is slightly tricky, as no picture will nicely reveal what we want. Instead we must realize that if a picture of S_1 with finite cone points shows any region of the two triangles outside of S_1, then the interiors of the faces must lie entirely outside S_1, since we understand the intersections of these faces with the sphere.

Figure 3.15 shows us both faces in black and the entire sphere S_1 in gray using Projection II, so that all cone points are finite. If the black faces were inside the sphere, then this picture would show them fully surrounded by gray arc. We can clearly see, however, that some of the black surfaces remain totally separated from the gray sphere. This suggests that the last supposition of the lemma holds.

3.6 The S_0 Intersections

We proceed similarly on the S_0 case, giving a lemma and then offering evidence that the conditions of the lemma are satisfied. As before we denote the topological ball S_0bounds by S_0°.

Lemma 3.6.1. *Suppose we have the following information about the intersections of $C_0 \to p_{102}$ and $C_2 \to p_{102}$ with S_0*

- *$(C_0 \to p_{102}) \cap S_0$ contains an $\mathbb{C}$-arc, C_0 short, joining v_0 and v_2.*
- *$(C_2 \to p_{102}) \cap S_0$ contains the vertex v_0.*
- *$(C_0 \to p_{102}) - \{C_0 \text{ short}\}$ is disjoint from S_0.*
- *$(C_2 \to p_{102}) - \{v_2\}$ is disjoint from S_0*
- *$C_0 \to p_{102}$ and $C_2 \to p_{102}$ are disjoint from S_0°*

Then our octahedron is disjoint from S_0°.

Proof. The last condition of the lemma establishes that $C_0 \to p_{102}$ and $C_2 \to p_{102}$ lie in the complement of S_0°. As the symmetries of the octahedron do not send $\partial\mathbb{C}H^2 - \{S_0^\circ\}$ to S_0°, the remaining faces must also be disjoint from S_0°. □

First we must note that C_0 *short* lies on one of our faces and the equator of S_0, giving us one $\mathbb{C}$-arc intersection. Also v_0 is an endpoint of C_2 *short*and lies on C_0, hence on S_0. Since p_{102} is not a cone point of S_0, we expect no $\mathbb{R}$-arc intersections. We proceed to show the remaining three conditions of the lemma in subsections.

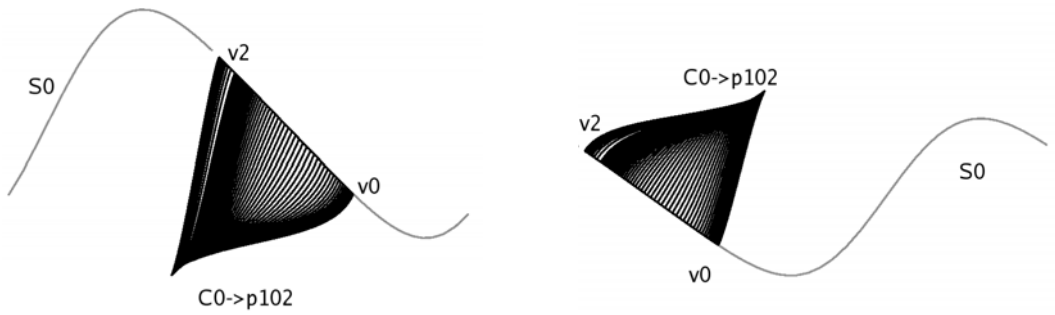

(a) **(b)**

Figure 3.16: $C_0 \to p_{102}$ with the p_{012} half (a) and the p_{021} (b) of S_0

3.6.1 $C_0 \to p_{102} - \{C_0 \ \ short\}$

We analyze the intersection of $C_0 \to p_{102} - \{C_0 \ \ short\}$ with the two halves of S_0 separately. Figures 3.16 (a) and (b) each show half of the sphere, drawn in gray and the face $C_0 \to p_{102}$ drawn in black. Figure 3.16 (a) employs Projection V, so this entire half of the sphere is coned to infinity. The black surface always remains underneath the gray arc in this image, and the gray arc covers the base of the black surface since they intersect along that portion of C_0.

Figure 3.16 (b) uses Projection IV to cone the other half of S_0 to infinity. Again we see that the black surface does not cross the gray arc, always remaining above it. Combining the information gleaned from these pictures, we can see that $C_0 \to p_{102}$ intersects S_0 only along the short half of C_0.

3.6.2 $C_2 \to p_{102} - \{v_2\}$

Turning our attention to $C_2 \to p_{102}$ and S_0, we analyze Figures 3.17 (a) and (b). Both of these images use Projection V and show S_0 in gray. 3.17 (a) allows

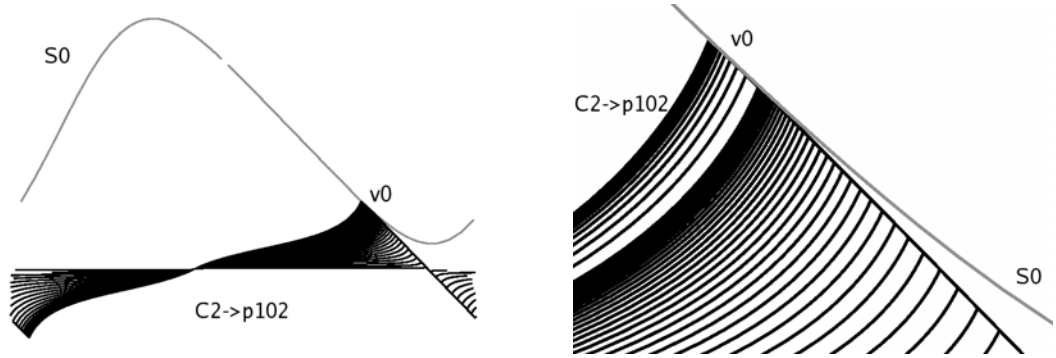

(a) **(b)**

Figure 3.17: $C_2 \to p_{102}$ with the p_{012} half of S_0 (a) and the region near v_0 (b)

us to see that the black surface remains underneath the gray arc outside of a neighborhood of v_0. Figure 3.17 (b) gives a better picture of the behavior near v_0, confirming that the black arcs do not cross the S_0.

We study the intersection behavior of this face with the other half of S_0 in Figures 3.18 (a) and (b). As in 3.17, we cone this half of S_0 to infinity, this time using Projection VI, and draw it in gray. Figure 3.18 (a) suggests that the black surface is always above the gray arc, but the behavior near v_0 is questionable. Figure 3.18 (b) provides greater detail of this region, showing that the black surface does not cross. This shows that there is reason to believe that the only intersection of $C_2 \to p_{102}$ with S_0 is the point v_0.

3.6.3 Disjointness from S_0°

Next, we show that the two faces are outside S_0 just as we did in the last section. Figure 3.19 is in Projection I and depicts S_0 in gray with neither cone point mapped to infinity. The cone point of our faces, shown in black, is mapped to infinity and thus the black arcs radiate away from the sphere. The aim of this

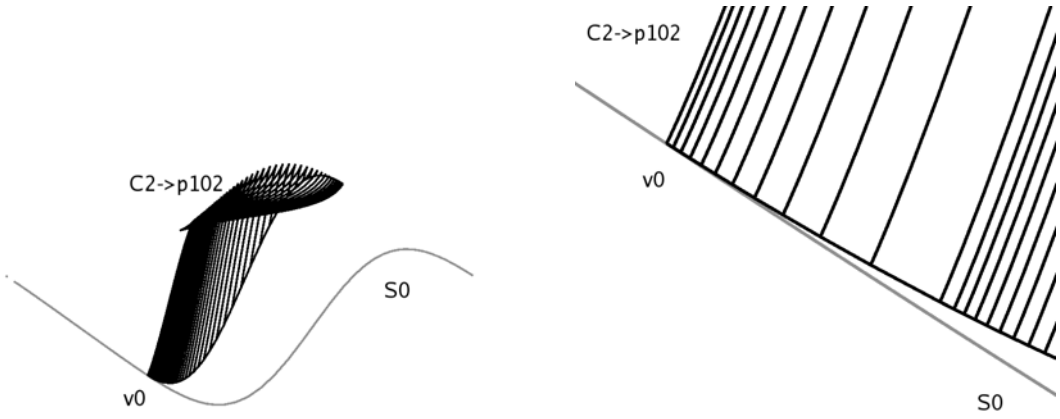

(a) **(b)**

Figure 3.18: $C_2 \to p_{102}$ with the p_{021} half of S_0 (a) and the region near v_0 (b)

picture is to establish that the gray sphere does not surround the black surfaces. Accordingly, we can say with confidence that the faces of our octahedron do not intersect the interior of S_0, having already established their intersections with the sphere itself.

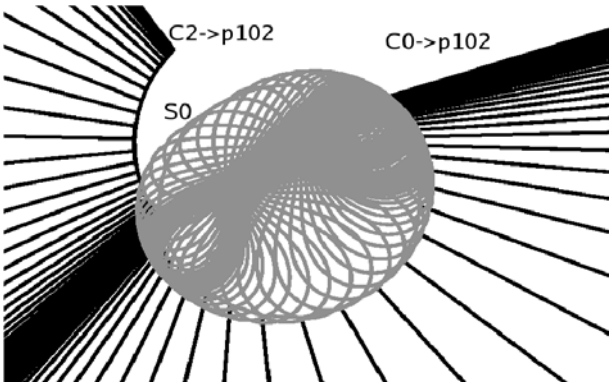

Figure 3.19: S_0 in gray and the two faces in black

3.7 The S_2 Intersections

The intersections of our faces with S_2 are slightly different from the other two spheres. In particular, the face $C_2 \to p_{102}$ is part of S_2, so its intersection behavior is already known. We give the following shorter lemma to deal with $C_0 \to p_{102}$

Lemma 3.7.1. *Suppose we have the following information about the intersections of $C_0 \to p_{102}$ with S_2*

- *$(C_0 \to p_{102}) \cap S_2$ contains an $\mathbb{R}$-arc, R, joining v_0 and p_{102}.*
- *$(C_0 \to p_{102}) - \{R\}$ is disjoint from S_2.*
- *$C_0 \to p_{102}$ is disjoint from S_2°*

Then our octahedron is disjoint from S_2°.

Proof. As we know the sphere S_2 is embedded, and $C_2 \to p_{102}$ is on S_2, we can conclude that $C_2 \to p_{102}$ is disjoint from S_2°. The conditions of the lemma give us the same result for $C_0 \to p_{102}$. As the octahedral symmetries do not send $\partial\mathbb{C}H^2 - \{S_2^\circ\}$ to S_2°, the remaining faces will be disjoint from S_2°. □

$C_0 \to p_{102}$ has one common $\mathbb{R}$-arc with S_2, arising from the shared points v_0 and p_{102}, so the first supposition is valid. We treat the second and third suppositions in the following subsections.

3.7.1 $C_0 \to p_{102}$ and S_2

We begin by analyzing images of $C_0 \to p_{102}$ and the p_{012} half of S_1.

Figures 3.20 (a) and (b) are in Projection II, so the arcs of the gray surface are coning to infinity. The image on the left shows the triangle $C_2\ long \to p_{012}$ in

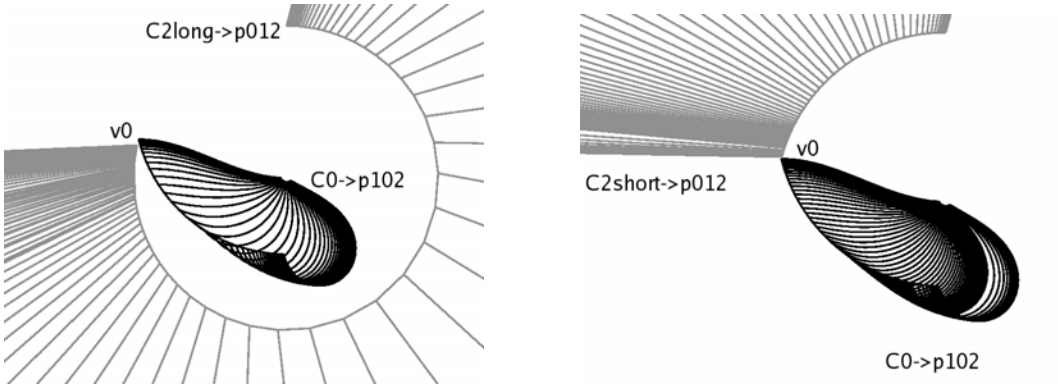

(a) **(b)**

Figure 3.20: $C_0 \to p_{102}$ with the long triangle (a) and the short triangle (b) from the p_{012} half of S_2

gray, and clearly displays that the two surfaces converge near v_0 but are otherwise quite distinct. Figure 3.20 (b) depicts C_2 *short* $\to p_{012}$ in gray, again displaying that the two surfaces do not intersect away from v_0. These images suggest that $C_0 \to p_{102} - \{R\}$ is disjoint from the p_{012} half of S_2.

For the other half of S_2, we need only look at C_2 *long* $\to p_{102}$, since we C_2 *short* $\to p_{102}$ is a face of our octahedron and its intersections have already

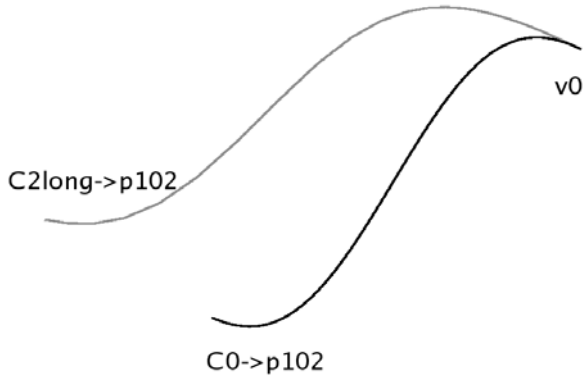

Figure 3.21: $C_0 \to p_{102}$ with the long triangle from the p_{102} half of S_2

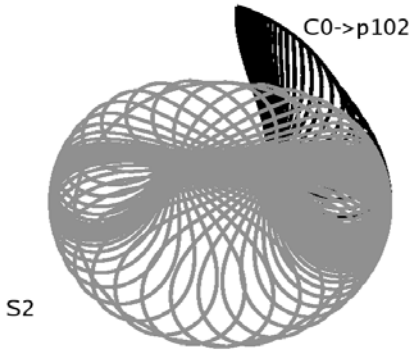

Figure 3.22: S_2 in gray and the face in black

been studied. Figure 3.21 shows C_2 *long* $\to p_{102}$ in gray and $C_0 \to p_{102}$ in black using Projection IV. Since both arcs are coning to infinity and the image is in cylindrical coordinates we do not see either surface. Nonetheless, the displayed arcs seem to remain disjoint until their point of intersection, v_0. It is likely that the only intersection of $C_0 \to p_{102}$ and S_2 is the $\mathbb{R}$-arc from v_0 to p_{102}.

3.7.2 Disjointness from S_0°

Finally we show evidence that part of the face $C_0 \to p_{102}$ lies outside S_2. Figure 3.22 is in Projection II, so no cone points are mapped to infinity. It shows that part of $C_0 \to p_{102}$, in black, escapes S_2, in gray. Together with the earlier evidence of how the face intersects the sphere, it is reasonable to think that the $C_0 \to p_{102}$ lies outside of S_0°, as desired.

3.8 Summary of Evidence

We have presented the reader with evidence supporting the following conclusions:

- The octahedron formed by coning the edges of the quadrilateral defined by

C_0 *short*, $I_1(C_0$ *short*), C_2 *short*, *and* and $I_1(C_2$ *short*) to the fixed points p_{102} and p_{021} is embedded.

- Four of the faces of this octahedron lie in $S_1 \cup S_1^\circ$, and four are in $\partial\mathbb{C}H^2 - \{S_1^\circ\}$.

- This octahedron is disjoint from both S_0° and S_2°.

Chapter 4

Embedding a Tile

In this chapter we will prove some embedding results for the octahedron. We will use the four $\mathbb{C}$-arcs of the octahedron to decompose it into two embedded halves. We will then analyze the behavior near the vertices where the two halves are joined. First, we give some tools that will be useful in our discussions.

4.1 Points and Parameterizations

There are several calculations that require more concrete formulas for our structures. More information about these equations are available in [S0, Sections 2.3 and 2.4]. Throughout this section, we use Θ to denote the projection from $\mathbb{C}^{2,1}$ taking (w_1, w_2, w_3) to $(\frac{w_1}{w_3}, \frac{w_2}{w_3})$.

As stated in Chapter 1, two distinct points uniquely determine a $\mathbb{C}$-circle through them. However, parameterizing these circles simply requires a third point. We obtain this point by carefully combining the other two.

Lemma 4.1.1. *The projective image, $\Theta(\hat{w})$, of the point $\hat{w}$ is on the $\mathbb{C}$-circle through x_1, x_2 and is distinct from x_1 and x_2. Where*

$$\hat{w} = \cos(\frac{-\pi}{4})\frac{i}{\langle q_1, q_2\rangle}q_1 + \lambda \sin(\frac{-\pi}{4})q_2 \tag{4.1}$$

and

$$q_1 = x_1 + i\frac{\langle x_1, x_2\rangle}{\| \langle x_1, x_2\rangle \|}x_2 \qquad q_2 = x_1 - i\frac{\langle x_1, x_2\rangle}{\| \langle x_1, x_2\rangle \|}x_2 \quad \textit{and } \lambda \in \mathbb{R}$$

Proof. First we show that $\langle \hat{w}, \hat{w}\rangle = 0$, and thus that $w \in \partial\mathbb{C}H^2$. Note that

$$\langle q_1, q_1\rangle = 0 = \langle q_2, q_2\rangle$$

so we are left with only the middle terms. Computing these yields:

$$\begin{aligned}\langle \hat{w}, \hat{w}\rangle &= \lambda \sin(\frac{-\pi}{4})\cos(\frac{-\pi}{4})\frac{i}{\langle q_1, q_2\rangle}\langle q_1, q_2\rangle \\ &\quad +\lambda \sin(\frac{-\pi}{4})\cos(\frac{-\pi}{4})\frac{-i}{\langle q_2, q_1\rangle}\langle q_2, q_1\rangle \\ &= 0\end{aligned}$$

as desired. To show that w is on the $\mathbb{C}$-circle through x_1 and x_2, consider $\langle \hat{w}, y\rangle$ where y is the polar vector for this $\mathbb{C}$-circle. By construction, this will be a sum with terms of the form $a_j\langle x_i, y\rangle$. Since x_1 and x_2 lie on the $\mathbb{C}$-circle, each of these terms must be zero. Finally, w must be distinct from x_1 and x_2 because $\langle \hat{w}, x_i\rangle \neq 0$ by a quick calculation. This completes the proof. We find it convenient to set $\lambda = \frac{33}{10}$ □

In order to show that the $\mathbb{C}$-arcs form an embedded quadrilateral in Heisenberg space, we will need exact parameterizations for the arcs in cylindrical coordinates. Recall that the cylindrical projection sends (z, t) to $(arg(z), t)$. For a $\mathbb{C}$-circle K, we will need to associate several constants. First, let $P_C(z, t) = z$ be projection to the plane $\mathbb{C} \times 0$ in $\mathcal{H}$. Also let $P_R(z, t) = t$ denote the projection to the t-coordinate. Lastly, recall that if K is finite in $\mathcal{H}$, then K is an ellipse and $P_C(K)$ is a circle. Let k_0 denote the center of mass for this ellipse and let r be the radius of $P_C(K)$. Define:

$$A = 2|P_C(k_0)|^2 \quad B = P_R(k_0) \quad E = \frac{r^2}{|P_C(k_0)|^2} - 1 \quad \phi = \angle 0 P_C\vec{(}k_0)\mathbb{R}^+$$

Lemma 4.1.2. *Let K be a finite $\mathbb{C}$-circle in $\mathcal{H}$ that links the t axis. Then the image of K in the cylindrical projection of $\mathcal{H}$ is the graph of the function*

$$f(\theta) = B + A\sin(\theta - \phi)\left(\cos(\theta - \phi) + \sqrt{E + \cos^2(\theta - \phi)}\right) \tag{4.2}$$

Proof. Using Heisenberg isometries if necessary, we may assume that k_0 is equal to $(s, 0)$ with $s \in \mathbb{R}^+$. Accordingly, we assume that $B = 0 = \phi$. Now let (x, y) denote the point on P_C of K making an angle of θ with the positive $\mathbb{R}$-axis. K must lie in the contact plane at $(s, 0)$, so the lift of (x, y) will have height Ay. The form above then reduces to A times the expression for y from the simultaneous equations $x^2 + y^2 = r^2$ and $x = y\cot(\theta)$. □

This equation appeared originally in [S1, Lemma 2.3], and was discussed again in [FP, Section 4.2].

Additionally, we will make use of two parameterizations of circles in $\partial\mathbb{C}H^2$. The first is for a $\mathbb{C}$-circle.

Lemma 4.1.3. *Let X, Y, and Z be distinct points that lie on a common $\mathbb{C}$-circle. We may take lifts $\hat{X}$, $\hat{Y}$, and $\hat{Z}$ such that*

$$\langle \hat{X}, \hat{Z}\rangle = 1 = \langle \hat{Y}, \hat{Z}\rangle \quad \textit{and} \quad \langle \hat{X}, \hat{Y}\rangle = i$$

Next, let

$$W(t) = i\hat{X} + t\hat{Z} \tag{4.3}$$

Then $\Theta(W(t))$ with $t \in [0, 1]$ parameterizes the arc of the $\mathbb{C}$-circle through X and Y that avoids Z.

Proof. Computing $\langle W(t), W(t)\rangle$, it is apparent that $W(t)$ is on $\partial\mathbb{C}H^2$. Similarly, one can easily check that $\langle W(t), O\rangle$, where O is the polar vector for the desired $\mathbb{C}$-circle, is zero for all $t \in [0,1]$. □

The next parametrization is for an $\mathbb{R}$-circle in $\partial\mathbb{C}H^2$.

Lemma 4.1.4. *Let X, Y, and Z be distinct points that lie on a common $\mathbb{R}$-circle. We may take lifts $\hat{X}$, $\hat{Y}$, and $\hat{Z}$ such that*

$$\langle \hat{X}, \hat{Y}\rangle = \langle \hat{Y}, \hat{Z}\rangle = \langle \hat{Z}, \hat{X}\rangle = r \in \mathbb{R}$$

Let

$$U(t) = (1-t)\hat{X} + t\hat{Y} + (t^2 - t)\hat{Z} \tag{4.4}$$

Then $\Theta(U(t))$ with $t \in [0,1]$ parameterizes the arc of the $\mathbb{R}$-circle through X and Y that avoids Z.

Proof. This follows from the fact that the arc is given by the convex combination of X and Y in $\mathcal{H}$, for a suitable mapping of $\partial\mathbb{C}H^2$ to $\mathcal{H}$. □

4.2 The embedded $\mathbb{C}$-arcs

We will show in this section that the four $\mathbb{C}$-arcs of our octahedron form an embedded quadrilateral, Q. More specifically, we will show that this quadrilateral is embedded when viewed in cylindrical coordinates with p_{102} mapped to infinity. This result allows us to prove the following theorem.

Theorem 4.2.1. *Let Q be the quadrilateral formed by the $\mathbb{C}$-arcs of the octahedron. Let Σ_{102} be the result of coning each side of Q to p_{102} and Σ_{021} be the analogous surface for p_{021}. Then Σ_{102} and Σ_{021} are embedded Q-based pyramids and the octahedron equals $\Sigma_{102} \cup \Sigma_{102}$.*

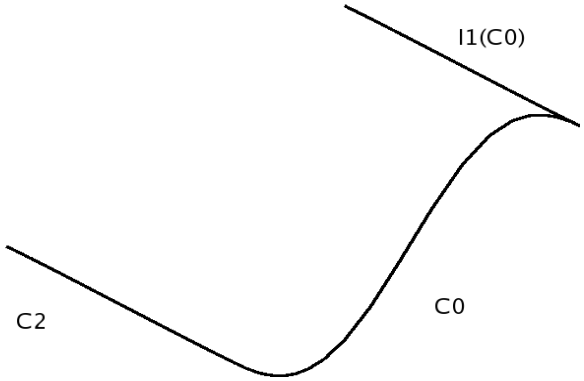

Figure 4.1: Three sides of Q

We will demonstrate that Σ_{102} is embedded and Σ_{021} will be embedded by symmetry. Q has six distinct pairs of sides to check for it to be embedded. The symmetries of the octahedron allow us to look at three representative pairs. Figure 4.1 will shows the three sides of Q that we will consider.

The first two of the three representative pairs do not require the explicit forms for their corresponding functions. The last pair will require them, however. Throughout this section, we will need to refer to a few angles. We list these below.

$$\theta_0 = Arg(P_C(v_0)) = \pi - \arctan(\sqrt{15}) \quad \theta_1 = Arg(P_C(v_1)) = 0$$
$$\theta_2 = Arg(P_C(v_2)) = \pi - \arctan(\frac{\sqrt{15}}{7})$$

We will also frequently refer to the function associated to an arc. Below is a list of functions and their corresponding arcs.

$$f(\theta) \leftrightarrow C_0 \quad g(\theta) \leftrightarrow C_2 \quad h(\theta) \leftrightarrow I_1(C_0)$$

4.2.1 C_0 and C_2

We find that C_0 *short* in cylindrical coordinates is the graph of $f(\theta)$ for $\theta \in [-\theta_0, \theta_0 + 2\pi]$. Similarly, C_2 *short* is the graph of $g(\theta)$ on $[\theta_1, -\theta_0]$ This is all we need to establish their intersection behavior

Lemma 4.2.1. *The graphs of $f(\theta)$ and $g(\theta)$ on $[0, \theta_0 + 2\pi]$ intersect only at $-\theta_0$.*

Proof. Computing $\theta_0 \approx -1.823$ shows that $0 = \theta_1 < -\theta_0 < \theta_0 + 2\pi < 2\pi$, so that C_0 *short* and C_2 *short* are graphed in the same period. Since they are defined on different domains elsewhere, the only possible intersection is at θ_0. Since the parametrization is accurate, the two graphs do intersect at θ_0. □

4.2.2 $I_1(C_0)$ and C_2

The graphs of $I_1(C_0)$ *short* and C_2 *short* should be completely disjoint. This is easy to see without knowing the explicit parametrization for either one.

Lemma 4.2.2. *The graphs of $g(\theta)$ and $h(\theta)$ corresponding to $I_1(C_0)$ short and C_2 short do not intersect.*

Proof. We compute $\theta_2 \approx 2.63623$ and find that $I_1(C_0)$ *short* is the graph of $h(\theta)$ for $\theta \in [\theta_2, \theta_0 + 2\pi]$. We have already established that C_2 *short* is the graph of $g(\theta)$ for $\theta \in [0, -\theta_0]$. Since $[0, -\theta_0] \cap [\theta 2, \theta_0 + 2\pi] = \emptyset$ and both intervals are contained in $[0, 2\pi]$, the graphs must be disjoint. □

4.2.3 C_0 and $I_1(C_0)$

These arcs present a greater challenge because their corresponding graphs are valued on overlapping intervals. We will show their intersection behavior in two steps, the first using concavity and the second using monotonicity.

We require the explicit formulation of both $h(\theta)$ and $f(\theta)$. Constructing additional points for each arc by the method of the previous section, we are able to compute the constants for the cylindrical parameterizations of the $\mathbb{C}$-arcs. Both of these formulations employ the parameterization of equation 4.2, found oringinally in [S0]. We first define $f(\theta)$.

$$f(\theta) = \frac{8}{9} sin(\theta - \pi) \left(cos(\theta - \pi) + \sqrt{\frac{3}{2} + cos^2(\theta - \pi)} \right) \quad for \quad \theta \in [-\theta_0, \theta_0 + 2\pi] \tag{4.5}$$

Next we give the constants required for $h(\theta)$.

$$\phi = \arctan(\frac{12335\sqrt{6} + 16268\sqrt{15}}{146412 + 22203\sqrt{10}}) \quad A = \frac{1}{3} \quad E = 9 \quad B \approx 1.93649$$

We approximate B here for brevity, but its exact value is easily deduced. $I_1(C_0)$ *short* is then the graph of $h(\theta)$ given by

$$h(\theta) = B + \frac{1}{3} sin(\theta - \phi) \left(cos(\theta - \phi) + \sqrt{9 + cos^2(\theta - \phi)} \right) \tag{4.6}$$

for $\theta \in [\theta_2, \theta_0 + 2\pi]$, where $\theta_2 = \pi - \arctan(\frac{\sqrt{15}}{7})$ as before. We may now state our result.

Lemma 4.2.3. *The graphs of $f(\theta)$ and $h(\theta)$ for $\theta \in [\theta_2, \theta_0 + 2\pi]$ intersect only at $\theta_0 + 2\pi$.*

Proof. The graphs are known to intersect at $\theta_0 + 2\pi$ by their construction. This leaves us to determine the behavior on $[\theta_2, \theta_0 + 2\pi)$. We will accomplish this in two steps.

Case 1 $(\pi+\phi, \theta_0+2\pi)$ First, we analyze the graphs on $(\pi+\phi, \theta_0+2\pi)$. We will need information about the second derivatives for f and h. We provide $f''(\theta)$ below. We do not give $h''(\theta)$ due to its length, but it is of similar form.

$$f''(\theta) = \frac{4\sin\theta(27\sqrt{2}+26\sqrt{2}\cos 2\theta - 36\eta\cos\theta - 4\eta\cos 3\theta + 2\sqrt{2}\cos 4\theta}{9(4+\cos 2\theta)^{\frac{3}{2}}} \quad where\ \eta = \sqrt{4+\cos 2\theta} \tag{4.7}$$

We compute that $h''(\theta) = 0$ and $f''(\theta) = 0$ at $\theta = \pi+\phi \approx 3.56$ and $\theta = \pi$, respectively. Also we observe that these are the unique zeroes of the second derivatives on $[\pi+\phi, \theta_0+2\pi]$ and that it has no singularities. Next we compute $f''(\theta_0+2\pi)$ and $h''(\theta_0+2\pi)$, approximating for brevity

$$f''(\theta_0+2\pi) \approx -1.44591 \quad h''(\theta_0+2\pi) \approx 0.206559$$

We may then safely conclude that

$$f''(\theta) < 0 \quad and \quad h''(\theta) > 0 \quad for \quad \theta \in (\pi+\phi, \theta_0+2\pi] \tag{4.8}$$

Since f is concave down on this interval and h is concave up, $h(\theta) > f(\theta)$ for $\theta \in (\pi+\phi, \theta_0+2\pi)$.

Case 2 Next we consider the interval $[\theta_2, \pi+\phi]$. We compute that the zeroes of $h'(\theta)$ on $[0, 2\pi]$ occur at

$$2\pi - 2\arctan(\sqrt{\frac{6-\sqrt{11}}{5}}) + \phi \quad and \quad 2\arctan(\sqrt{\frac{6-\sqrt{11}}{5}}) + \phi$$

Neither of these points lies in $[\theta_2, \pi+\phi]$. Also, $h'(\pi+\phi) < 0$, so $h(\theta)$ must be decreasing for all $\theta \in [\theta_1, \pi+\phi]$. Hence, the global minimum of $h(\theta)$ on this interval is $h(\pi+\phi)$.

Performing a similar computation, we find the zeroes of $f'(\theta)$ occur at:

$$2\pi - 2\arctan(\sqrt{\frac{9+2\sqrt{14}}{5}} \quad and \quad 2\arctan(\sqrt{\frac{9+2\sqrt{14}}{5}}$$

Both of these values lie outside $[\theta_2, \pi+\phi]$. We also note that $f'(\pi+\phi) > 0$, so that f must be increasing on this interval. We can conclude that the global maximum of $f(\theta)$ on this interval occurs at $f(\pi+\phi)$. Approximating for brevity, we obtain

$$\begin{aligned} f(\theta) < f(\pi+\phi) \approx 0.8606630 < 1.93649 \approx h(\pi+\phi) < h(\theta) \\ for \quad \theta \in [\theta_1, \pi+\phi] \end{aligned} \tag{4.9}$$

Statements 4.6 and 4.7 taken together prove the lemma.

□

As stated, these three lemmas together with the octahedral symmetries show that the quadrilateral is embedded in cylindrical coordinates. Since the $\mathbb{R}$-arcs of Σ_{102} are straight lines perpendicular to Q in this perspective, we know that Σ_{102} is embedded. Symmetry gives the same result for Σ_{021} and thus proves the theorem.

4.3 Behavior Near the Vertices

We now consider what happens near a vertex of Q when we join Σ_{102} and Σ_{021}. There are four vertices of Q, but only two up to symmetry. We choose v_0 and v_2 as representatives. At each of these vertices there are (up to symmetry) three pairs of faces we must consider. We obtain the following results

Statement 4.3.1. *Modulo roundoff error, The following pairs of faces in* $\Sigma_{102} \cup \Sigma_{021}$ *are embedded in a neighborhood of* v_0*.*

- $C_0 \to p_{102}$ *and* $C_2 \to p_{021}$
- $C_0 \to p_{021}$ *and* $C_2 \to p_{102}$
- $C_0 \to p_{021}$ *and* $C_0 \to p_{102}$

Statement 4.3.2. *Modulo roundoff error, there is a neighborhood of* v_2*, and a neighborhood of* v_1*, where the following two pairs of faces are embedded.*

- $C_0 \to p_{102}$ *and* $I_1(C_0) \to p_{021}$
- $C_0 \to p_{102}$ *and* $C_0 \to p_{021}$

Statement 4.3.1 and symmetry assert that, modulo roundoff error, $\Sigma_{102} \cup \Sigma_{021}$ is embedded in a neighborhood of v_0 and in a neighborhood of $I_1(v_0)$. We will prove each theorem in a different subsection.

4.3.1 Methods

Let K be a $\mathbb{C}$-arc with an endpoint v and (E, q) be a flag. Let T be the surface formed from K via the coning process for (E, q). We wish to approximate T near v.

Recall that we may take a Heisenberg stereographic projection sending q to ∞ and E to the t-axis in $\mathcal{H}$. The $\mathbb{C}$-circle containing K will be an ellipse in $\mathcal{H}$ under this map. Accordingly, there is some smooth parameterization of K, $g(r) : [0, 1] \to \mathbb{R}^3$ with $g(0) = v$. Also recall the $\mathbb{R}$-arcs of T will be lines with constant t value in $\mathcal{H}$.

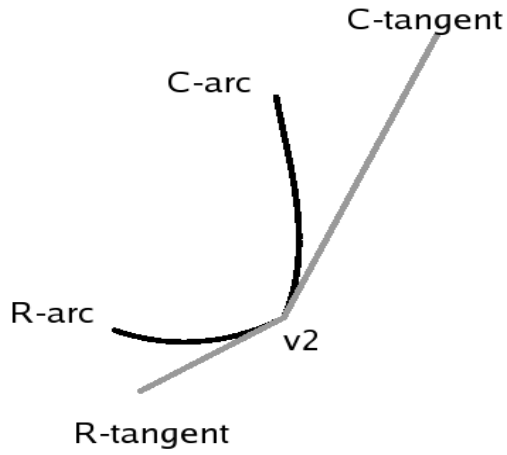

Figure 4.2: Two arcs and their tangent vectors

Now define $F(r,s) : [0,1] \times [1,\infty) \to \mathcal{H}$ by $F(r,s) = (sg_1(r), sg_2(r), g_3(r))$, where g_i is the ith component function of g. Observe that F parameterizes the surface T and is differentiable at v. As a result, the tangent plane at v is well defined. It is spanned by the vectors $\frac{\partial F}{\partial r}$ and $\frac{\partial F}{\partial s}$ evaluated at $(0,1)$. These are the tangent vectors at v to the $\mathbb{C}$-arc, K, and the $\mathbb{R}$-arc of T joining v and q.

We can then conclude that a first order approximation to T near v is given by the positive span, denoted $span_+$ of the tangent vectors at v to the $\mathbb{C}$-arc and the $\mathbb{R}$-arc based at v. Given two faces, we will compare their approximations to determine if there is a non-trivial intersection. If the approximations associated to a pair of faces have no improper intersections, we may conclude that there is a neighborhood of the vertex where the two faces are embedded. Figure 4.2 shows two arcs based at v_2 in black and their tangent vectors in gray. The picture was made in Mathematica using the projection $(z,t) \mapsto z$. The approximating surface in this case would be the positive span of the gray vectors.

4.3.2 Near v_0

We will prove Statement 4.3.1 by considering the approximating surfaces for the three pairs of faces at v_0. The result follows for $I_1(v_0)$ by symmetry.

We parameterize the $\mathbb{C}$-arcs and the $\mathbb{R}$-arcs based at v_0 by equations 3 and 4 in section 1. Due to the nature of the calculations, it was impractical to find exact values for the tangent vectors. There are four tangent vectors we associate to v_0, we label them W_C, W_R, Y_C, and Y_R. The subscripts indicate whether the vector is tangent to a $\mathbb{C}$-circle or an $\mathbb{R}$-circle. We list the values of these vectors in ambient coordinates for S^3 before proceeding.

$$\begin{aligned} W_C &\approx (-0.0980843,\ 0.633131,\ -0.0980843,\ 0.633131) \\ W_R &\approx (-0.0419263, 0.270633, 0.0419263, -0.270633) \\ Y_C &\approx (0,\ 0,\ 0.000171704,\ -0.00110834) \\ Y_R &\approx (-0.314447,\ 0.297696,\ 0.314447,\ -0.297696) \end{aligned} \tag{4.10}$$

We begin with the pair $C_0 \to p_{102}$ and $C_2 \to p_{021}$.

Lemma 4.3.1. *There is a neighborhood of v_0 where $C_0 \to p_{102}$ and $C_2 \to p_{021}$ intersect only at v_0.*

Proof. The vectors Y_C and Y_R are the tangent vectors to the initial $\mathbb{C}$-arc and $\mathbb{R}$-arc of $C_2 \to p_{021}$. Similarly, the tangent vectors associated to $C_0 \to p_{102}$ are W_C and W_R. We approximate the two faces near v_0 by $span_+(Y_C, Y_R)$ and $span_+(W_C, W_R)$. We compute the dependencies of the four vectors to obtain:

$$-0.000875287W_C + 0.00204769W_R = Y_C \tag{4.11}$$

Since the left hand side is not in $span_+(W_C, W_R)$, we see that the approximating surfaces do not intersect. This proves the lemma. □

Next we look at $C_0 \to p_{021}$ and $C_2 \to p_{102}$. This involves the same collection of vectors with the same dependencies as the previous case, just in a different arrangement. Now the vectors W_C and Y_R correspond to $C_0 \to p_{102}$, while Y_C and W_R are with $C_2 \to p_{021}$. We obtain a similar result.

Lemma 4.3.2. *There is a neighborhood of v_0 where $C_0 \to p_{021}$ and $C_2 \to p_{102}$ intersect only at v_0.*

Proof. Rearranging equation 4.8 , we have

$$-Y_C + 0.00204769W_R = 0.000875287W_C \tag{4.12}$$

Which proves the lemma. □

Lastly we consider the pair $C_0 \to p_{021}$ and $C_0 \to p_{102}$. These faces share a $\mathbb{C}$-arc, so we have only three tangent vectors to consider, W_C, W_R, and Y_R. The two faces have disjoint interiors in a neighborhood of v_0 if $aW_C + bW_R + cY_R = 0$ has no nontrivial solution.

Lemma 4.3.3. *There is a neighborhood of v_0 where $C_0 \to p_{021}$ and $C_0 \to p_{102}$ have disjoint interiors.*

Proof. The two faces have disjoint interiors in a neighborhood of v_0 if $aW_C + bW_R + cY_R = 0$ has no nontrivial solution. We find that $Y_R \notin span(W_C, W_R)$, completing the proof. □

The three lemmas together prove the statement.

4.3.3 Near v_2

We repeat the same analysis for v_2 to prove Statement 4.3.2. This result is not as strong as Theorem 4.1. We believe the stronger result to be true, but the nature of their intersection makes one pair significantly harder to show. We again associate four vectors to v_2, E_C, E_R, D_C, and D_R. We list their approximate values

$$\begin{aligned} E_C &\approx (-0.0112009,\ -0.0723015,\ -0.0112009,\ -0.0723015) \\ E_R &\approx (0.0419263,\ 0.270633,\ -0.0419263,\ -0.270633) \\ D_C &\approx (-0.0336027,\ -0.216905,\ 0.0112009,\ 0.0723015) \\ D_R &\approx (-0.209631,\ -0.487139,\ 0.209631,\ 0.487139) \end{aligned} \tag{4.13}$$

In this case, the E vectors come from $C_0 \to p_{102}$ and the D vectors correspond to $I_1(C_0) \to p_{021}$. As before, we obtain our desired result.

Lemma 4.3.4. *There is a neighborhood of v_2 where $C_0 \to p_{102}$ and $I_1(C_0) \to p_{021}$ intersect only at v_2.*

Proof. Solving the system yields the following equation.

$$E_C - 0.534314E_R = D_C \tag{4.14}$$

This shows that the approximating surfaces intersect only at v_2. □

Finally, we consider the faces $C_0 \to p_{102}$ and $C_0 \to p_{021}$. Near v_2, their approximating surfaces are given by $span_+(E_C, E_R)$ and $span_+(E_C, D_R)$. We show that they intersect only along their common $\mathbb{C}$-arc.

Lemma 4.3.5. *There is a neighborhood of v_2 where $C_0 \to p_{102}$ and $C_0 \to p_{021}$ have disjoint interiors.*

Proof. As equation 4.11 shows, D_R is not in $span(E_C, E_R)$. □

The two lemmas suffice to prove the statement.

Appendix A

Appendix - Recreating Figures

We offer the reader the shorthand described in chapter 2 for recreating the images in chapter 3.

Figure 3.2 (a)

I_0 to p_{102}, short	I_2 to p_{012}, short
-	2
black	black
black	black
I_0 to p_{021}, short	I_2 to p_{021}, short
1	1
black	black
black	black
I_1 to p_{102}, short	I_1 to p_{102}, long
-	-
gray	gray
gray	gray

Figure 3.3

I_0 to p_{102}, short	I_2 to p_{021}, short
-	21
black	gray
black	gray

Figure 3.4

I_0 to p_{102}, short	I_0 to p_{021}, short
-	-
black	gray
black	gray

Figure 3.5

I_0 to p_{102}, short	I_0 to p_{021}, short
-	1
black	gray
black	gray

Figure 3.6

I_0 to p_{102}, short	I_2 to p_{012}, short
-	2
black	gray
black	gray

Figure 3.7 (a)

I_0 to p_{102}, short	I_2 to p_{021}, short
-	1
black	gray
black	gray

Figure 3.7 (b)

I_0 to p_{021}, short	I_2 to p_{021}, short
-	21
black	gray
black	gray

Figure 3.8

I_0 to p_{021}, short	I_0 to p_{021}, short
1	-
gray	black
gray	black

Figure 3.9

I_0 to p_{102}, short	I_0 to p_{102}, short
-	1
black	gray
black	gray

Figure 3.10 (a)

I_0 to p_{102}, short	I_2 to p_{021}, short
-	-
black	gray
black	gray

Figure 3.10 (b)

I_0 to p_{021}, short	I_2 to p_{012}, short
-	2
black	gray
black	gray

Figure 3.12 (a)

I_0 to p_{102}, short	I_1 to p_{102}, long
-	1
black	gray
black	gray

Figure 3.12 (b)

I_0 to p_{102}, short	I_1 to p_{102}, short
-	1
black	gray
black	gray

Figure 3.13

I_2 to p_{012}, short	I_1 to p_{102}, long
2	1
black	gray
black	gray

Figure 3.14

I_2 to p_{012}, short	I_1 to p_{102}, short
2	1
black	gray
black	gray

Figure 3.15

I_0 to p_{102}, short	I_2 to p_{012}, short
-	2
black	black
black	black
I_1 to p_{102}, short	I_1 to p_{102}, long
-	-
gray	gray
gray	gray
I_1 to p_{102}, short	I_1 to p_{102}, long
1	1
gray	gray
gray	gray

Figure 3.16 (a)

I_0 to p_{102}, short	I_0 to p_{021}, short
-	0
black	gray
black	gray
I_0 to p_{021}, long	
0	
gray	
gray	

Figure 3.16 (b)

I_0 to p_{102}, short	I_0 to p_{021}, short
-	-
black	gray
black	gray
I_0 to p_{021}, long	
-	
gray	
gray	

Figure 3.17

I_2 to p_{012}, short	I_0 to p_{021}, short
2	0
black	gray

black	gray
I_0 to p_{021}, long	
0	
gray	
gray	

Figure 3.18

I_2 to p_{012}, short	I_0 to p_{021}, short
2	-
black	gray
black	gray
I_0 to p_{021}, long	
-	
gray	
gray	

Figure 3.19

I_0 to p_{102}, short	I_2 to p_{012}, short
-	2
black	black
black	black
I_0 to p_{021}, long	I_0 to p_{021}, short
-	-
gray	gray

gray	gray
I_0 to p_{021}, short	I_0 to p_{021}, long
0	0
gray	gray
gray	gray

Figure 3.20 (a)

I_0 to p_{102}, short	I_2 to p_{012}, long
-	-
black	gray
black	gray

Figure 3.20 (b)

I_0 to p_{102}, short	I_2 to p_{012}, short
-	-
black	gray
black	gray

Figure 3.21

I_0 to p_{102}, short	I_2 to p_{012}, long
-	2
black	gray
black	gray

Figure 3.22

I_0 to p_{102}, short

-

black

black

I_2 to p_{012}, short

-

gray

gray

I_2 to p_{012}, short

2

gray

gray

I_2 to p_{012}, long

-

gray

gray

I_2 to p_{012}, long

2

gray

gray

BIBLIOGRAPHY

[FP] E. Falbel and J. Parker *The Moduli Space of the Modular Group in Complex Hyperbolic Geometry*, Invent. Math., **152** (2003), 57-78.

[Ga] J. Wyss-Gallifent, *Discreteness and Indiscreteness Results for Complex Hyperbolic Triangle Groups*, Ph.D. Thesis, University of Maryland (2000).

[Go] W.M. Goldman, *Complex Hyperbolic Geometry*, Oxford University Press, (1999).

[GP] W.M. Goldman and J. Parker, *Complex Hyperbolic Ideal Triangle Groups*, J. reine agnew Math.,**425** (1992) 71-86.

[S0] R.E. Schwartz, *Ideal Triangle Groups, Dented Tori, and Numerical Analysis*, Annals of Math,**153** (2001) 533-598.

[S1] R.E. Schwartz, *A Better Proof of the Goldman-Parker Conjecture*, Geometry and Topology, (Vol. 9) (2005) 1539-1601.